# Classifying Magnetosheath Jets using MMS - Statistical Properties

**Savvas Raptis[1], Tomas Karlsson[1], Ferdinand Plaschke[2], Anita Kullen[1], Per-Arne L. Lindqvist[1]**

[1]Space and Plasma Physics, School of Electrical Engineering and Computer Science, KTH Royal Institute of Technology, Stockholm, Sweden
[2]Space Research Institute, Austrian Academy of Sciences, Graz, Austria

**Key Points:**

- Magnetosheath jets' properties exhibit differences depending on $\theta_{Bn}$.
- Classification of jet database based on $\theta_{Bn}$, using MMS data is presented.
- All classes show different properties with some classes being compatible with existent generation mechanisms.
- Bow shock ripple mechanism and SLAMS are generally supported by statistical properties.

Corresponding author: Savvas Raptis, `savvra@kth.se`

**Abstract**

Using Magnetospheric Multiscale (MMS) data, we find, classify and analyze transient dynamic pressure enhancements in the magnetosheath (jets) from May 2015 until May 2019. A classification algorithm is presented, using in-situ MMS data to classify jets ($n = 8499$) into different categories according to their associated angle between IMF and the bow shock normal vector ($\theta_{Bn}$). Jets appearing for $\theta_{Bn} < 45$ are referred to as quasi-parallel, while jets appearing for $\theta_{Bn} > 45$ as quasi-perpendicular jets. Furthermore, we define those jets that occur at the boundaries between quasi-parallel and quasi-perpendicular magnetosheath as boundary jets. Finally, encapsulated jets are jet-like structures with similar characteristics to quasi-parallel jets while the surrounding plasma is of quasi-perpendicular nature.

We present the first statistical results of such a classification and provide comparative statistics for each class. Furthermore, we investigate correlations between jet quantities. Quasi-parallel jets have the highest dynamic pressure while occurring $\sim 5 - 10$ times more frequently than quasi-perpendicular jets. The infrequent quasi-perpendicular jets, have a much smaller duration, velocity, and density and are therefore relatively weaker. We conclude that quasi-parallel and boundary jets have similar properties and are unlikely to originate from different generation mechanisms. Regarding the encapsulated jets, we suggest that they are a special subset of quasi-parallel jets originating from the flanks of the bow shock, under dominant $B_y$ IMF. Our results support existing generation theories, such as the bow shock ripple and SLAMS-associated mechanisms while indicating that other factors may contribute as well.

## 1 Introduction

The magnetosheath plasma can have strong fluctuations in velocity, density and associated magnetic field. These fluctuations are the result of short time scale variations of the IMF and the resulting bow shock geometry. A key component that influences the level of fluctuation is the angle between the IMF and the bow shock normal vector ($\theta_{Bn}$). It has been shown that in the case of the quasi-parallel shock ($\theta_{Bn} < 45$) the downstream plasma is strongly turbulent whereas in the quasi-perpendicular shock ($\theta_{Bn} > 45$) there is a much smoother and calmer environment (Fuselier, 2013; Wilson III, 2016). The main reason the two regions have different characteristics is that in the quasi-parallel case, reflected ions can travel upstream along the magnetic field lines causing instabilities and associated wave growth. This creates a foreshock region characterized by a suprathermal ion distribution. This region is not present in the quasi-perpendicular case where the transition between upstream and downstream flow is distinct and straightforward (Schwartz & Burgess, 1991). As a result, in the quasi-perpendicular bow shock, there are much sharper and well-defined transitions between the upstream and downstream plasma.

Magnetosheath jets are local enhancements of dynamic pressure above the surrounding background level, reaching values even higher than the upstream solar wind. The dynamic pressure enhancements can be attributed to a density increase (Savin et al., 2008; Karlsson et al., 2012, 2015), to a velocity increase (Archer et al., 2012) or may result from an enhancement of both (Amata et al., 2011; Plaschke et al., 2013). These jets are mainly found behind the quasi-parallel bow shock and the current prominent creation theory is that they result from solar wind foreshock fluctuations interacting with the bow shock.

Many terms and definitions have been used in the literature to describe the jet phenomenon, as thoroughly discussed in the review paper by Plaschke et al. (2018). In principle, the jet determination can be done via two methods. The first one is by using a sliding average time window which indicates a background value on the magnetosheath dynamic pressure and search for enhancements that are 100% - 200% higher than that value. (Archer & Horbury, 2013; Gunell et al., 2014; Karlsson et al., 2015; Gutynska et al., 2015).

Another way is to apply a minimum threshold to the x component of the dynamic pressure to be at least 25% of the solar wind's associated dynamic pressure (Amata et al., 2011; Hietala et al., 2012; Plaschke et al., 2013). In this work we will use the term "magnetosheath jet" or "jet" to describe an enhancement in the dynamic pressure compared to the values of the background magnetosheath plasma, using a sliding time window.

The dynamic pressure enhancements can reach up to $\sim 15$ times of the background value. Their duration can be of the order of seconds, up to several minutes with an average of 30 seconds (Archer & Horbury, 2013). Parallel to the flow, the scale is $\sim 0.5$ $R_E$ and in the perpendicular direction slightly more at roughly $\sim 1$ $R_E$ (Archer & Horbury, 2013; Plaschke et al., 2018). While as mentioned above, jets' dynamic pressure enhancement is usually attributed to both density and velocity increase (Amata et al., 2011; Archer & Horbury, 2013), there are cases where some jets exhibit a density decrease. Specifically, Plaschke et al. (2013), found 10.5% of jets showing a density decrease. On the other hand, Archer et al. (2012) using a different jet criterion found up to 18% of jets exhibiting a density drop. Furthermore, jets can generate a vortical motion in the background magnetosheath plasma, causing a deceleration to the ambient plasma around the jet (Plaschke & Hietala, 2018). It has been recently shown that jets occur roughly 9 times more often downstream of the quasi-parallel bow shock compared to the quasi-perpendicular one (Vuorinen et al., 2019). This is in agreement with the observations showing low solar wind cone angles favoring the creation of subsolar magnetosheath jets, while other solar wind parameter variations have no significant effect (Plaschke et al., 2013).

Magnetosheath jets may have an important impact on the magnetosphere. Their increased momentum can create local deformation of the magnetopause and trigger local magnetic reconnection (Hietala et al., 2018), drive compressional waves (Plaschke & Glassmeier, 2011) or even cause direct plasma penetration in the magnetosphere (Karlsson et al., 2012). Furthermore, they can affect the radiation belts through the loss of outer belt electrons, (Turner et al., 2012; Xiang et al., 2016). Additionally, jets can affect the aurora via the mechanism of "dayside throat aurora" which has been connected to magnetosheath particle precipitation (Han et al., 2017; Wang et al., 2018). The link between jets and energy transfer through the magnetosphere was also observed recently when surface eigenmodes were found to be excited through a collision between a jet and the magnetopause (Archer et al., 2019). Finally, jet manifestation seems to be a universal phenomenon that is speculated to occur in other planetary (e.g. Mercury (Karlsson et al., 2016)) and astrophysical bow shocks (Giacalone & Jokipii, 2007; Plaschke et al., 2018).

### 1.1 Generation of jets

While the generation of jets is not yet fully explained, a prominent theory is that the majority of the jets are associated with ripples of the quasi-parallel bow shock. Hietala et al. (2009) and Hietala and Plaschke (2013) propose that through the interaction with a locally curved bow shock, plasma flows are less decelerated while still being compressed. This results in a relative velocity difference compared to the surrounding flow that gets more decelerated, explaining the dynamic pressure enhancement ("jet") observed in the magnetosheath region. A similar mechanism, where foreshock short large-amplitude magnetic structures (SLAMS) interact with the local bow shock ripples may be responsible for generating some jets. SLAMS (upstream pulsations) are typical phenomena in the quasi-parallel foreshock and have very large magnetic field amplitudes ($\sim 5$ times higher than the background) (Schwartz et al., 1992). Regarding jets, it has been suggested that jets associated with SLAMS can have a relative increase of density and magnetic field strength whereas the ones associated with purely bow shock ripple mechanism may be mainly velocity driven (Karlsson et al., 2015). Furthermore, there have been recent simulations supporting the creation of a SLAMS-like subset of jets (Palmroth et al., 2018).

Another theory associates the creation of jet-like transient phenomena with IMF rotational discontinuities. Early simulations have shown that pressure pulses may be generated when there is a switch between quasi-perpendicular and quasi-parallel bow shock or vice versa (Lin et al., 1996). Later, Archer et al. (2012) found several jets that were consistent with this picture by using upstream and downstream solar wind data while Karlsson et al. (2018) investigated the anatomy of some typical cases that exhibit a magnetic field rotation in the magnetosheath.

Additional mechanisms have been suggested, involving solar wind discontinuity-related spontaneous hot flow anomalies (SHFAs) resulting from foreshock cavitons (Zhang et al., 2013; Omidi et al., 2013). Retinò et al. (2007), connected magnetic reconnection inside the magnetosheath with local particle acceleration which could appear as jets. This mechanism, however, is not sufficient to explain jets with velocities much greater than the local Alfvén speed (Archer et al., 2012). Other proposed mechanisms describe the jet phenomenon in terms of a slingshot effect (Chen et al., 1993; Lavraud et al., 2007). This effect attributes the velocity enhancement of jets to a release of magnetic tension of a flux tube along the flanks.

There is no consensus regarding which of the above theories is responsible for the origin of jets. Furthermore, there has been no investigation regarding statistical differences that may arise in the properties of the jets depending on the angle between the IMF field and the bow shock normal vector. In this work, we address both of these knowledge gaps by defining different classes of jets, and investigating their statistical properties to give insight into how likely each generation mechanism is for each class.

### 1.2 Different Types of Jets

Using MMS data we identify and classify the jets into 4 main categories. Jets have been observed for over 20 years now behind the quasi-parallel bow shock (Němeček et al., 1998). It is believed that the majority of jets are occurring in a quasi-parallel configuration and therefore the first category we search for are the ”Quasi-parallel (Qpar) jets”. As a complementary category, we are investigating cases of jets that are behind the quasi-perpendicular bow shock that we call ”Quasi-perpendicular (Qperp) jets”. Furthermore, we classified jets that are found at the boundary between a Qpar and a Qperp geometry or vice versa. Our goal is to investigate if these jets are connected to the mechanism proposed by Archer et al. (2012), and we call them ”Boundary jets”. It has been hypothesized that maybe these jets are different than the other classes and may hold separate properties (Archer et al., 2012; Archer & Horbury, 2013; Karlsson et al., 2018). Finally, after inspecting the derived dataset, we introduce a category called ”Encapsulated jets”. These jets contain plasma with very similar characteristics to Qpar, while the surrounding plasma is of Qperp nature.

Apart from the main categories, in our jet database, we include 2 more classes. The first are the ones that were identified as jets, but were not automatically classified by our algorithm by not fulfilling all necessary criteria. These jets therefore, remain as ’Unclassified jets’ until further inspection. Secondly, jets found very close to either the bow shock or the magnetopause (’Border jets’) are not investigated in this work to exclude possible edge effects.

## 2 Data

In this study, we use data starting from the 1st of September 2015 until the 1st of May 2019. For the measurements that characterize the jets in the magnetosheath, we use data from the MMS (Magnetospheric Multiscale) mission, while for the upstream values of the solar wind we use data primarily from the ACE (Advanced Composition

Explorer) mission. The measurements used for both solar wind and magnetosheath regions are presented in Geocentric Solar Ecliptic (GSE) coordinates.

### 2.1 MMS - Magnetosheath Data

For magnetic field measurements, we use the fluxgate magnetometer (FGM) (Russell et al., 2016) which has a resolution of 1/0.125 sample/sec in the slow survey mode. Furthermore, we use the fast plasma investigation (FPI) (Pollock et al., 2016) which has a time resolution of 4.5 seconds for ion measurements. Finally, for determining the position of MMS, the Magnetic Ephemeris Coordinates (MEC) data that are included in the MMS dataset are used (Burch et al., 2016).

During their orbit, the MMS spacecraft are regularly traversing the magnetosheath region. The small separation of the four MMS spacecraft allows us to only use data from MMS1 for the purposes of this paper.

### 2.2 OMNIweb/ACE - Solar Wind Data

For parts of our analysis, we use upstream solar wind measurements, publicly available through the 1 minute resolution OMNI database. This dataset is created using multiple spacecraft measurements (primarily ACE & Wind (Stone et al., 1998)) and is smoothed and time-shifted to the nose of the Earth's bow shock. The bow shock location changes according to the solar wind parameters and is automatically adjusted for every time-shifted measurement (King & Papitashvili, 2005). The time resolution of the OMNIweb high-resolution database is 1 data point per minute. To associate OMNIweb data to the jets we took average solar wind values of a 15 minute window, starting 10 minutes before the jet's observation time and up to 5 minutes after. This value seemed to provide accurate results in the cases that we tested manually, and was done to compensate for several possible errors that are explicitly analyzed in the method section below.

## 3 Method

### 3.1 Magnetosheath Identification

We begin by identifying time intervals when MMS is in the magnetosheath region. The determination of each region (magnetosheath/solar wind/magnetosphere) is done based on manually derived thresholds for ion number density ($n_i$), velocity ($V_i$), temperature ($T_i$), and flux ($F_i$). Furthermore, we require three (3) sequential data points to be classified as a different region in order to change the region's characterization (e.g. from the magnetosheath to solar wind). This was done to avoid cases where due to the variance of the measurements, one point might be misclassified as another region. Finally, we impose a minimum duration for each region to be 15 minutes. Smaller regions were considered to be possibly influenced by bow shock or magnetopause crossings.

### 3.2 Jet Determination

For jet determination we rely on local magnetosheath data. Doing so, we increase our dataset sample size by not limiting our observations to time periods where upstream solar wind data are available. We found that roughly $\sim 27\%$ of the jets contained unreliable measurements (NaN values) in their corresponding solar wind dynamic pressure. As a result, the choice of local MMS measurements for jet determination appears to be superior regarding the size of the derived dataset.

For our initial dataset, we impose a minimum relative dynamic pressure threshold which defines a jet as a time interval when the dynamic pressure is at least twice as large as a 20-min average value. Specifically, we use:

**Table 1.** Initial dataset of the magnetosheath jets for the period 10/2015 - 04/2019.

| Subset | Number (n) | Percentage (%) | Criteria |
|---|---|---|---|
| All | 16034 | 100 | Eq. (1) |
| Combined | 8499 | 53 | Eqs. (1), (3) |
| High energy | 4369 | 27 | Eqs. (1), (3), (4) |

$$P_{msh} \geq 2\langle P_{msh}\rangle_{20\,\mathrm{min}} \tag{1}$$

where,

$$P_{msh} = m_p n_i V_i^2 \tag{2}$$

and angular brackets denote an averaging by a 20 min sliding window. When magnetosheath regions are less than 20 minutes, the average window is taken to be equal to the whole region.

We then implement an additional criterion, combining all the jets that have a shorter time separation than 60 seconds from each other.

$$t_{start,i+1} - t_{end,i} \geq 60\mathrm{s} \tag{3}$$

Where $i = 1, 2, 3...n$ is the number of the jet in the database.

This was done based on the assumption that jets with such a small time separation are part of the same fast plasma flow. A similar technique is also applied when studying fast plasma flows that occur in the plasma sheet, known as bursty bulk flows (BBFs) (Angelopoulos et al., 1994). Furthermore, not combining jets may lead to skewed statistics since not combining jets can result in an artificially increased number of jets with much shorter duration and similar properties, possibly causing misleading results.

Finally, for the sake of completeness, we create a subset of high dynamic pressure jets by imposing an absolute thresholds to the maximum dynamic pressure measured within the jet period.

$$P_{dyn,max} \geq 2\ \mathrm{nPa} \tag{4}$$

The resulting initial dataset is shown in Table 1.

After obtaining the jet dataset as shown in Table 1, we implement an automatic classification scheme in order to create a subset of jets for each class. The classification scheme is based on applying several thresholds, trials, schemes and time adjustments to the original dataset. The algorithm includes 6 stages of classification that are implemented sequentially. Stages can hold up to three different quality levels and up to 6 trials of time adjustment. The purpose of this method is to increase the number of jets that are classified after every stage while only slightly increasing the misclassification cases. Afterwards, we choose the stages and conditions and stop when the misclassification becomes too large.

**Table 2.** Properties of the four main classes of jets.

| Name | Characteristics |
|---|---|
| Quasi-parallel | High energy flux, low anisotropy, high magnetic field variance |
| Quasi-perpendicular | Low energy flux, high anisotropy, low magnetic field variance |
| Boundary | Switch between Qpar characteristics to Qperp or Vice Versa |
| Encapsulated | Switch from Qperp characteristics to Qpar and back to Qperp |

In the following subsections, we will briefly explain some key ideas and components regarding our classification scheme, while more details can be found in Appendix A and Appendix B.

### 3.3 Jet Classification

For the jet classification, we use MMS data with solar wind data acting as an extra quality measure when available. Like our jet determination algorithm, the classification code avoids the use of solar wind measurements. This was done for several reasons. The values available are measured from $L_1$ and are time-lagged to the bow shock introducing an error from the artificial propagation to the bow shock nose. The generated error in such time-lagging procedure can reach values up to 30 minutes (Mailyan et al., 2008; Case & Wild, 2012), while producing large uncertainty in short time scale phenomena (e.g. rotations of magnetic field). Furthermore, the available measurements are averaged to 1 minute, which makes certain short time scale features impossible to detect. Additionally, the jets are identified throughout the whole magnetosheath region, meaning that one has to time-shift the associated solar wind values after the bow shock interaction, differently for each jet, in order to accurately characterize the jets, providing additional uncertainty to the measurements. Finally, for roughly 1/4 of the jets IMF measurements were not available. All the above reasons led us to primarily use magnetosheath data rather than solar wind for our classification.

We classify the jets based on MMS measurements in the magnetosheath. It has been shown that the quasi-parallel (Qpar) magnetosheath has different properties than the quasi-perpendicular (Qperp) magnetosheath. Specifically, in Qpar magnetosheath, temperature anisotropy is typically different compared to the Qperp one (Anderson et al., 1994; Fuselier et al., 1994). Furthermore, stronger fluctuations in the plasma density, velocity, and the magnetic field have been associated with Qpar magnetosheath (Formisano & Hedgecock, 1973; Luhmann et al., 1986). Finally, the most striking difference is a distinct high energy ion population that can be observed in the Qpar magnetosheath (Gosling et al., 1978; Fuselier, 2013). Therefore, the classification code works by applying manually derived thresholds to the ion energy flux, temperature anisotropy and magnetic field variance.

The characteristics of the 4 main classes of jets are summarized in Table 2.

In order to verify that we can accurately distinguish between Qpar and Qperp magnetosheath we checked the measurements of MMS when it was close to the subsolar point of the bow shock. Due to the proximity to the subsolar point, there is a smaller error in the propagation of the solar wind measurements to the bow shock, and a shorter distance for the plasma flow to propagate inside the magnetosheath. Therefore, we can confirm the expected characteristics of the magnetosheath plasma. An example of such a test can be seen in Figure 1. In this example, we calculate the cone angle defined as:

$$\theta_{cone} = \arccos\left(\frac{|B_x|}{|B|}\right) \tag{5}$$

which in the case of subsolar point it is identical to $\theta_{Bn}$ since the bow shock normal vector $\hat{n}$ is pointing on the x direction.

As we can see in Figure 1, there are distinct magnetosheath characteristics associated with the quasi-parallel and quasi-perpendicular bow shock. The high energy ion flux is the one that is most visible, while the temperature anisotropy and the magnetic field variance are also clearly correlated. The exact computation of these quantities can be found in Appendix A. Interestingly, the region which is not shaded with any color is a typical example where the high resolution measurements of MMS provide evidence of a short-time scale change of IMF while the cone angle measurements of 1-min resolution fully miss the rapid change that is seen in the magnetosheath.

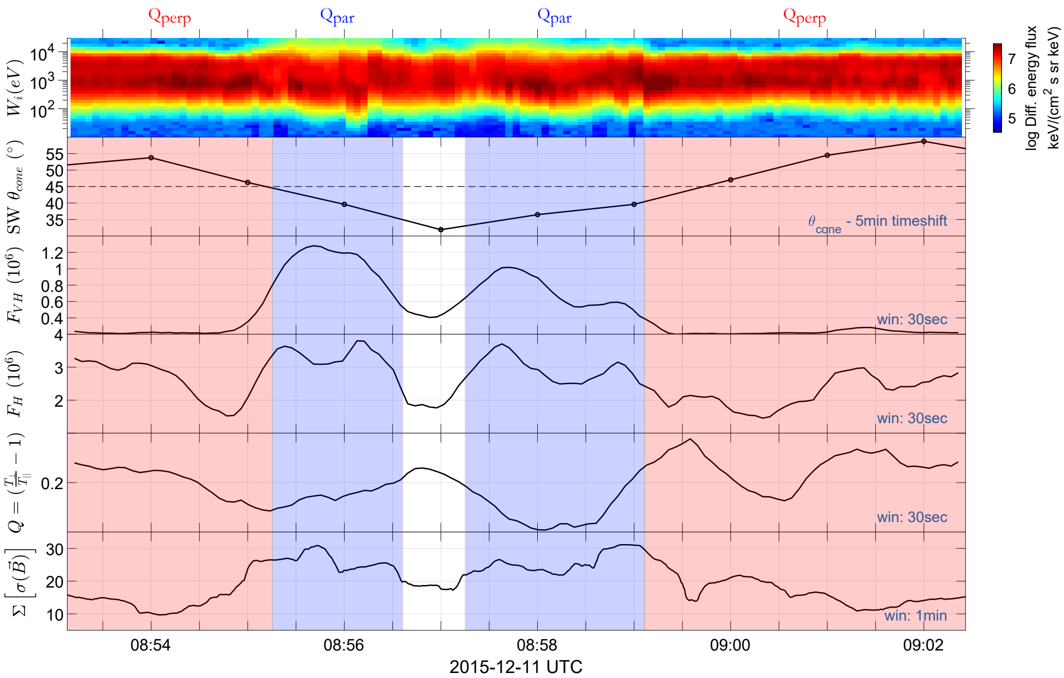


**Figure 1.** Visualization of associated changes between Qpar and Qperp magnetosheath. From top to bottom, ion energy spectrum, solar wind cone angle, very high energy ($16 - 28$ keV) differential ion flux, high energy ($7 - 12$ keV) differential ion flux, temperature anisotropy, and sum of the magnetic field standard deviation. Blue shaded region represent Qpar regions while red show Qperp ones. More information about the computation of each quantity can be found in Appendix A.

Typical examples of each jet class can be seen in Figure 2. In Figure 2(a), we show a quasi-parallel jet whereas in Figure 2(b) a quasi-perpendicular one. A boundary jet can be seen in Figure 2(c) and finally an encapsulated one in Figure 2(d).

#### *3.3.1 Pre-jet and Post-jet Periods*

Our scheme is based on the assumption that there are three distinct phases in the jet phenomenon. Since the jet crosses MMS, observations include the plasma environment propagating in front of the jet, the jet flow and the plasma behind the jet. We call these plasma environments, pre-jet, jet and post-jet periods.

The jet period is the duration in which the criterion of Eq. (1) is satisfied. In the case that the jet contains only one data point, we re-adjust the starting and ending point of the jet to include one extra data point before and after the jet respectively. The pre-jet period is a period of time before the actual jet which is usually characterized by a gradual increase in dynamic pressure. The post-jet period is an approximately equally long period of time, characterized by a gradual drop of dynamic pressure associated with a non-jet magnetosheath region.

The pre/post-jet time periods are set based on jet duration as:

$$\Delta t_{pre,post} = \begin{cases} 45\,\text{sec}, & \Delta t_{jet} < 45\,\text{sec} \\ 60\,\text{sec}, & 45\,\text{sec} \leq \Delta t_{jet} < 75\,\text{sec} \\ 75\,\text{sec}, & \Delta t_{jet} \geq 75\,\text{sec} \end{cases} \tag{6}$$

It was decided to have the pre/post jet time increasing with jet duration mainly to assist the classification routine which is categorizing data points and chooses the class of the jet based on the percentage of them that fit certain criteria. Furthermore, by manually inspecting cases of extensive duration jets ($\Delta t_{jet} > 45\,\text{sec}$) we found that a slight increase to their pre/post jet times made the classification algorithm more accurate.

#### *3.3.2 Verification and Validation of Data Set*

In order to determine the optimal settings for our classification scheme, we created a test data set through visual inspection, containing jets of every class. After testing the accuracy of our classification procedure we have chosen the optimal stage from which the output was sufficient to derive statistical results and the number of misclassification cases was limited (Appendix B).

As a final validation of our dataset, we visually inspected the results of certain unclassified, boundary and encapsulated jets and re-classified manually a few misclassifications that the automatic procedure produced ($\sim 10-20\%$). This resulted in some slight changes while ensuring that the accuracy of our classification is satisfactory. Typically, the majority of automatic misclassifications were either between boundary and unknown or encapsulated and unknown. This was expected since these classes had much more precise criteria to be met both in the jet and in the surrounding plasma region.

More information regarding the verification of the data set and the accuracy determination of our procedure can be found in Appendix B.

The number of jets in the final classified dataset is shown in Table 3.

The jet position for the main classes is shown in Figure 3. There, the MMS position at the time of observation of the maximum dynamic pressure is shown. The magnetopause and bow shock regions are plotted based on the model and the typical conditions found in Chao et al. (2002).

### 3.4 Derived quantities

In order to derive statistical results for each of the jet classes, we mainly use the ”best cases” listed in Table 3. These met all criteria from the automatic procedure and have also been manually verified. As a result, unless explicitly mentioned, we only use the verified (”best”) cases for our analysis. Finally, when we are referring to ”main” classes we mean the four classes described in Table 2.

**Table 3.** Classified dataset of the magnetosheath jets for the period 09/2015 - 04/2019. Using as initial dataset the combined ($n = 8499$) jets of Table 1. The properties of each class are shown in Table 2.

| Subset | Number | Percentage (%) |
|---|---|---|
| Quasi-parallel | 2284 | 26.9 |
| Best cases | **860** | 10.1 |
| Quasi-perpendicular | 504 | 5.9 |
| Best cases | **211** | 2.5 |
| Boundary | 744 | 8.8 |
| Best cases | **154** | 1.8 |
| Encapsulated | 77 | 0.9 |
| Best cases | **57** | 0.7 |
| Other | 4890 | 57.5 |
| Unclassified/Uncertain | 3499 | 41.2 |
| Border | 1346 | 15.8 |
| Data Gap | 45 | 0.5 |

For all the jets, we investigate the minimum, mean and maximum values of their properties. We also examine how these quantities are distributed compared to the background magnetosheath plasma. As a result, we introduce "difference" values, referring to quantities that are either maximum, mean, or minimum within a jet from which we subtracted a 5-minute background magnetosheath value.

$$\Delta X_{(max/mean/min,5)} = X_{max/mean/min} - \langle X \rangle_{5min} \tag{7}$$

In the background value ($\langle X \rangle_{5min}$), we remove the jet period. As a result,

$$\langle X \rangle_{5min} = \frac{1}{2n} \sum_{i}^{n} (X_{t_{start}-i} + X_{t_{end}+i}) \tag{8}$$

Where start/end is the starting and ending point of the jet period, and $n = 33$ measurements.

The differences between the mean and max values were, statistically speaking, insignificant due to the short duration of the jets. Therefore, in order to make the visualization easier, we have chosen to show mainly the maximum values. Moreover, to avoid the few cases where the average values were contaminated by solar wind or magnetopause measurements, we pick the background values to be 5 minutes. It should be noted that the "difference" values (Eq. (7)) can give insight in the cases of Qpar and Qperp jets but should be treated with caution when referring to boundary and encapsulated jets. The reason is that the background normalization in the first two cases is being done with plasma which is more or less similar throughout the 5 minute period that was taken. On the other hand, for the boundary and encapsulated cases, due to the nature of plasma being different between the jet and the surrounding measurements, the difference values can be unreliable.

To determine the distance of each jet from the bow shock we generate a bow shock model for every jet based on its associated solar wind values. The average associated solar wind conditions are derived from values 10 min before the jet and up to 5 minute after. The asymmetric usage of measurements before and after the jet was done to com-

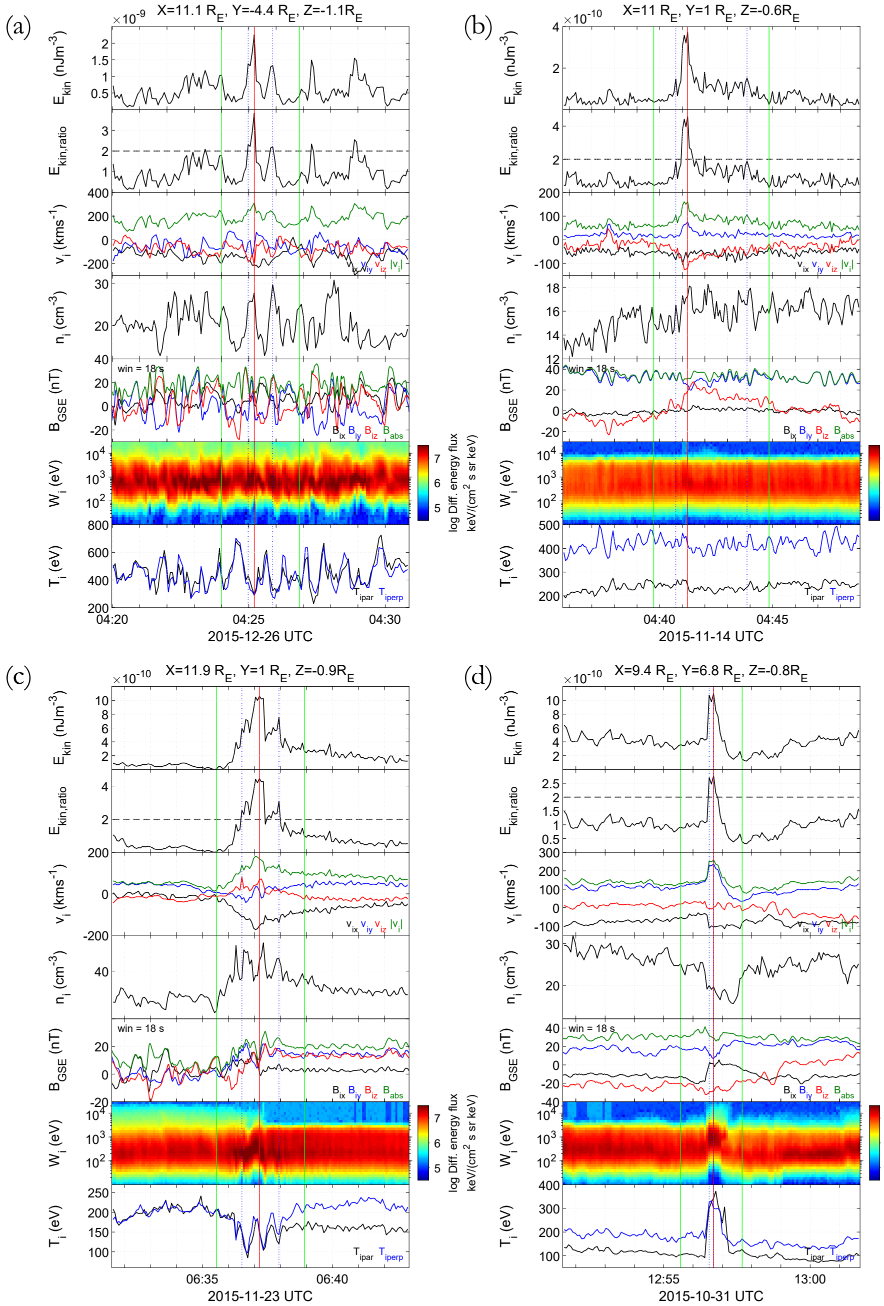


**Figure 2.** Examples of the four main categories of jets. (a): Quasi-parallel, (b): Quasi-perpendicular, (c): Boundary, and (d): Encapsulated jet. From top to bottom, in each subplot: dynamic pressure, ratio of the dynamic pressure to the background level, ion velocity, ion number density, magnetic field components averaged with a moving window of 18 seconds, ion energy spectrum and parallel and perpendicular components of ion temperature. The red vertical line shows the time of maximum dynamic pressure, blue vertical lines the jet period, and green vertical lines indicate the pre-jet the and post-jet times. Finally, the black dotted line on the second panel of every subplot indicates a 200% enhancement of dynamic pressure compared to the background.

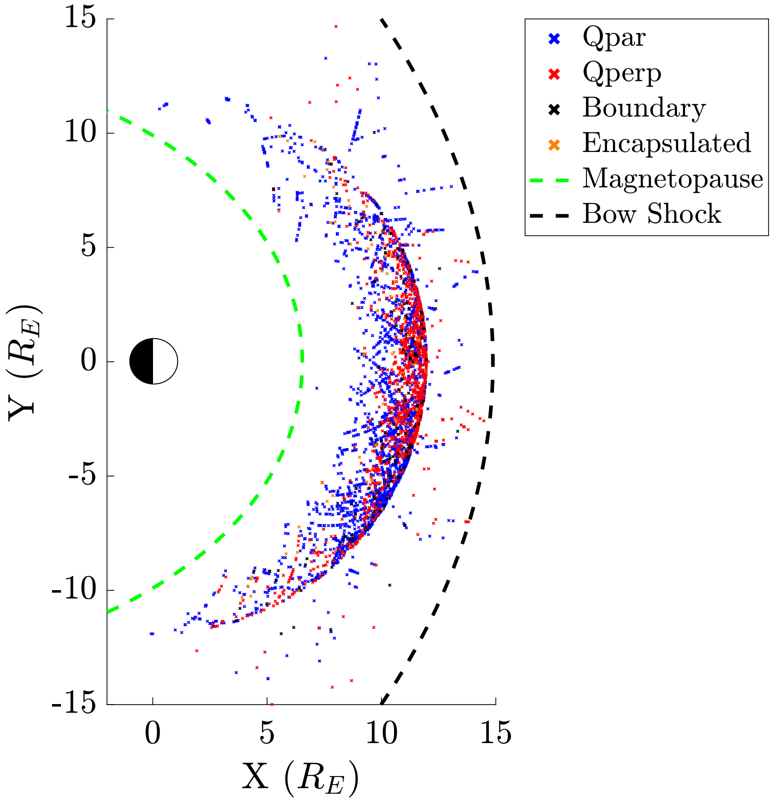


**Figure 3.** Location of the 4 magnetosheath jet classes projected to the $xy$-plane in GSE coordinates, identified in MMS data between May 2015 and May 2019. The green and black dashed lines mark the approximate location of the magnetopause and the bow shock during average solar wind conditions. Coordinate system is the Geocentric Solar Ecliptic (GSE) and both axes are normalized to Earth radius ($R_E = 6.371$ km).

pensate for the time plasma takes to travel from the bow shock to the MMS position. Later, we use the maximum velocity vector ($\mathbf{V}_{max}$) of each jet to propagate it back in time until we cross the bow shock. This procedure took $\Delta T_{BS_i}$ time for each jet ($i$) which was calculated by the amount of steps multiplied by the time resolution of the FPI instrument (4.5 seconds). After we have approximated a point of origin for each jet, we compute the distance from the bow shock as:

$$\Delta X = X_{BS} - X_{MMS} \tag{9}$$

Where $X$ can be radial distance ($R$), distance along the $yz$ plane ($\rho$), or distance along the $x$ axis ($X$). It should be noted, that the theoretical position of the bow shock may have a significant error as shown in several works (e.g. (Merka et al., 2003; Turc et al., 2013) and therefore any statistical results should be considered with caution.

Furthermore, our algorithm which computed the point of origin for each jet, assumes that no breaking nor change in the direction of the jet occurred from its creation until its observation by MMS. This assumption is certainly not correct and it produced several cases where the jet was found to originate from a totally non-physical origin ($\Delta R > 30R_E$). In these cases, we used the dominant component of the velocity to propagate the jet to the bow shock as an alternative option. However, there were cases that there were still unphysical results. In these cases, we simply removed the jet at this specific analysis. This procedure reduced the number of jets in all classes slightly ().

Throughout the text, when we refer to subsolar jets we apply an extra criterion on the jets that are classified to one of the main classes:

$$\begin{aligned} |Y_{GSE}| &< 2\mathrm{R_E} \\ |Z_{GSE}| &< 2\mathrm{R_E} \end{aligned} \tag{10}$$

Where $|Y_{GSE}|$ and $|Z_{GSE}|$ are the absolute value of the $y$ and $z$ coordinate of the MMS satellite at the time of maximum dynamic pressure of each jet. Applying this criterion generated a smaller subset of jets ($n = 298$). This set is used to investigate relations between distances from the bow shock. We do so because a jet close to a subsolar position with a dominant $x$ velocity component is more likely to have travelled a distance approximately equal to the $x$ distance between MMS and the bow shock.

To investigate the orientation of the flow, we calculate two more quantities. First, we calculate the velocity in the $yz$ plane ($V_\rho$), and then the angle between that velocity velocity and the $x$ axis. The velocity $V_\rho$ is defined as:

$$V_\rho = \sqrt{V_y^2 + V_z^2} \tag{11}$$

While the angle is defined as:

$$\theta_{V_\rho} = \arctan\left(\frac{V_\rho}{|V_x|}\right) \tag{12}$$

An interesting quantity is the angle between the magnetic field vector before and after the jet. This was done in order to search for any interesting properties that could link a jet class to the pressure pulses connected to rotational discontinuities that were first described by Archer et al. (2012).To calculate the magnetic field angle we took the average of the magnetic field vector for 30 sec, 1 min and 2 min before and after the jet and determined the angle between the "averaged" magnetic field measurements. All the derived quantities provided similar average and median results, although the actual values varied slightly. We have decided to use the 30 sec averaged magnetic field for the computation of the presented magnetic field angle.

$$\theta_B = \arccos\left(\frac{\langle\mathbf{B}\rangle_{\Delta t_1} \cdot \langle\mathbf{B}\rangle_{\Delta t_2}}{|\langle\mathbf{B}\rangle_{\Delta t_1}||\langle\mathbf{B}\rangle_{\Delta t_2}|}\right) \tag{13}$$

Where $\Delta t_1$ is a 30 sec duration before the jet and $\Delta t_2$ a 30 sec duration after the jet.

Another quantity that is considered is the angle between the average velocity vector of the jet and the velocity vector of the surrounding plasma. This is done by taking the average vector of the jet period and finding its angle to the average velocity vector taken 5 minutes before and after the jet. In order to have a velocity that better characterized the background flow of the plasma, we removed 30 seconds before and after the jet when computing the average background velocity vector.

$$\theta_V = \arccos\left(\frac{\langle\mathbf{V}\rangle_{\Delta t_{jet}} \cdot \langle\mathbf{V}\rangle_{\Delta t_2}}{|\langle\mathbf{V}\rangle_{\Delta t_{jet}}||\langle\mathbf{V}\rangle_{\Delta t_2}|}\right) \tag{14}$$

Where, $\Delta t_{jet}$ is the jet period and $\Delta t_2$ is an 9-minute duration, of 4.5 minutes before $t_{1,start} - 30s$ and after $t_{1,end} + 30s$.

To investigate the total effect of each jet we calculated the integrated dynamic pressure over the jet's duration along the flow (total fluence) as:

$$f_{total} = \int P_{dyn} \cdot |\mathbf{V}| \cdot dt = \sum_{i}^{n} P_{dyn,i} \cdot |\mathbf{V}_i| \cdot \Delta t \tag{15}$$

Where, $n$ is the number of measurements within each jet period and $\Delta t$ is the time resolution of the FPI instrument (4.5 seconds).

We also present correlation coefficients between a number of jet properties. The most commonly used correlation coefficients are the Pearson's correlation coefficient (PCC) and Spearman's rank correlation coefficient ($\rho_{Sp}$). The former describes a possible linear relation between the two variables while the second is showing the strength of a monotonic relation (Myers et al., 2013). For our analysis, we use the Spearman's coefficient to determine correlations between jets' quantities.

Throughout the results section, all plots are color-coded the same way. Qpar jets are represented by blue, Qperp by red, boundary by black and encapsulated by orange.

## 4 Results

The first observation, as shown in Table 3, is that the number of jets found behind the quasi-parallel shock is significantly higher than the number found in other classes. Boundary jets seem to be quite common as well, while quasi-perpendicular jets are much less frequent and finally, encapsulated jets occur very rarely. While we cannot derive how frequently each jet occurs for each magnetosheath region (Qpar and Qperp), one can assume that on average the magnetosheath region during MMS orbits is equally distributed between the two regions. With that assumption, we can estimate that quasi-parallel jets occur much more frequently than quasi-perpendicular jets. Specifically, they can occur $\sim 5 - 10$ more often, depending on how many of the uncertain jets could be classified as Qpar jets (41.2% of the detected jets are unclassified, see Table 3). This result is in agreement with recent results showing that the frequency of Qpar jets can be $\sim 9$ higher than Qperp jets (Vuorinen et al., 2019).

### 4.1 Properties of the Jet Classes

In Figures 4 - 9, the basic properties of each class along with several quantities defined in the previous section are shown.

Starting with the basic properties of the jets in Figure 4, quasi-parallel and boundary jets have on average much higher dynamic pressure ($\langle P_{max} \rangle \sim 3$ nPa ) compared to the quasi-perpendicular jets ($\sim 0.5$ nPa), while encapsulated jets seem to lie somewhere in between. Similar differences between classes can be observed for the differences in dynamic pressure from the background magnetosheath plasma with or without solar wind normalization. The distributions and the average values of the absolute ion velocity show that the velocities of Qperp jets are much lower than these of Qpar, boundary and encapsulated jets. Interestingly, while this effect seems to hold regardless of the normalization technique, when normalizing to the solar wind, the difference in velocity between classes is reduced. This could mean that on average the velocity of a jet primarily depends on the solar wind velocity at the time of its creation. Furthermore, it shows that the majority of Qperp jets of our dataset are found under low solar wind velocities. Regarding the ion density, Qpar and boundary jets have on average twice as high density as the Qperp and encapsulated jets. When looking at the difference values however,

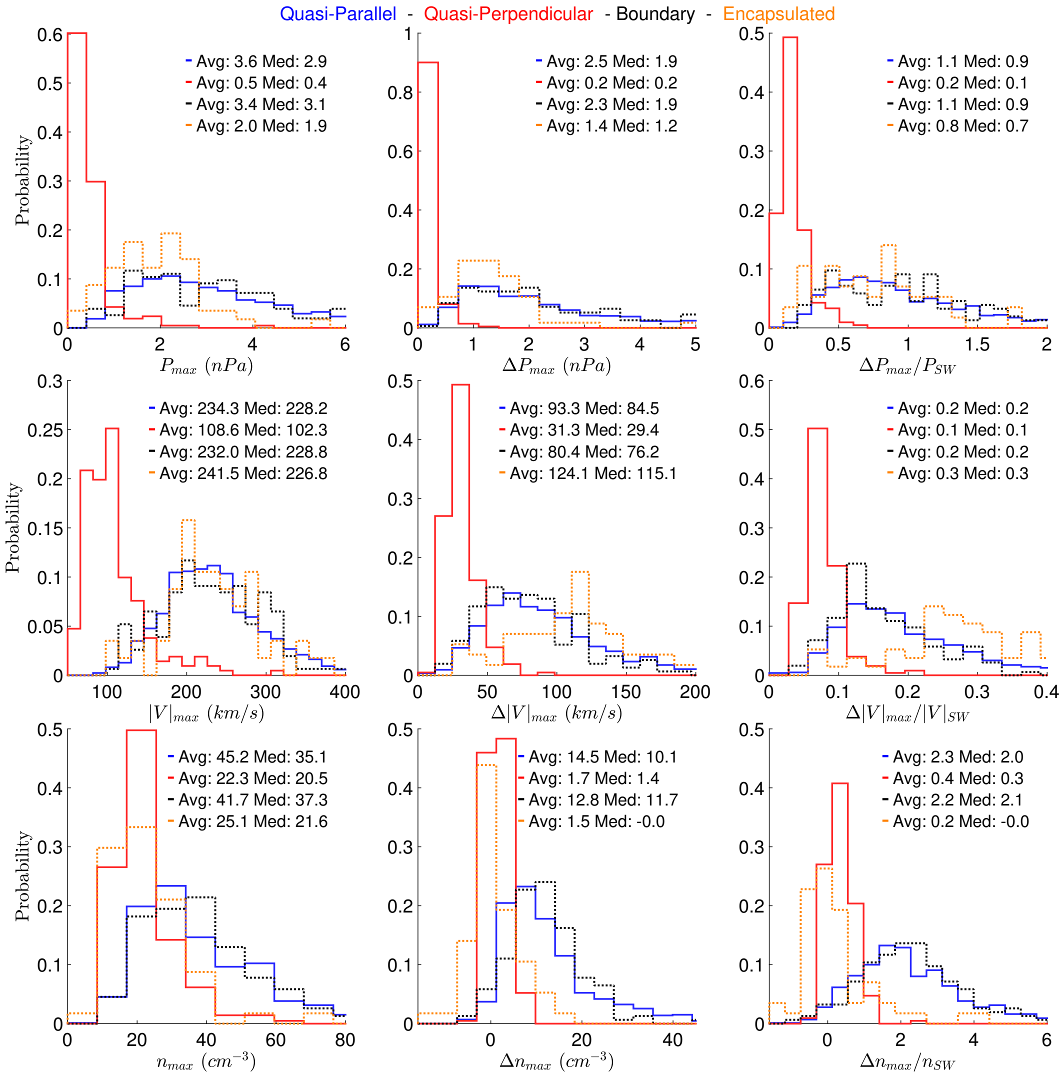


**Figure 4.** Histograms showing distributions, average and median values for the maximum values of the basic jet quantities. Maximum dynamic pressure, absolute velocity and density are shown. First columns show the measured values, the second describe the difference from the background and the third are normalized to the associated solar wind values.

the actual density gain is an order of magnitude more for the Qpar and boundary cases compared to the other two. Finally, the overall net gain of density and velocity for the jets is much higher for the rest of the classes compared to the Qperp jets.

In general, Figure 4 shows that the properties of Qpar and boundary jets are very similar, while both velocity and density changes in the Qperp jets are much smaller. This could imply differences in their generation mechanisms. Finally, encapsulated jets are dominated by an increase in velocity with absolute velocities gain being even higher than Qpar jets while their density distribution is very similar to Qperp jets.

For all jet classes, there are several jets where the dynamic pressure reaches values even higher than the dynamic pressure of the solar wind as expected from earlier studies (Plaschke et al., 2013). However, only very few cases of jets have a velocity higher than their associated solar wind velocity. These occurrences (mainly a few encapsulated jets) can be explained from certain observational biases and generation theories that are later presented and discussed. We can conclude that the main contribution of the dynamic pressure increase compared to the solar wind is due to the compression that solar wind undergoes after interacting with the bow shock. This, in turn, causes a density increase that can be of orders of magnitudes higher in the jets compared to the solar wind.

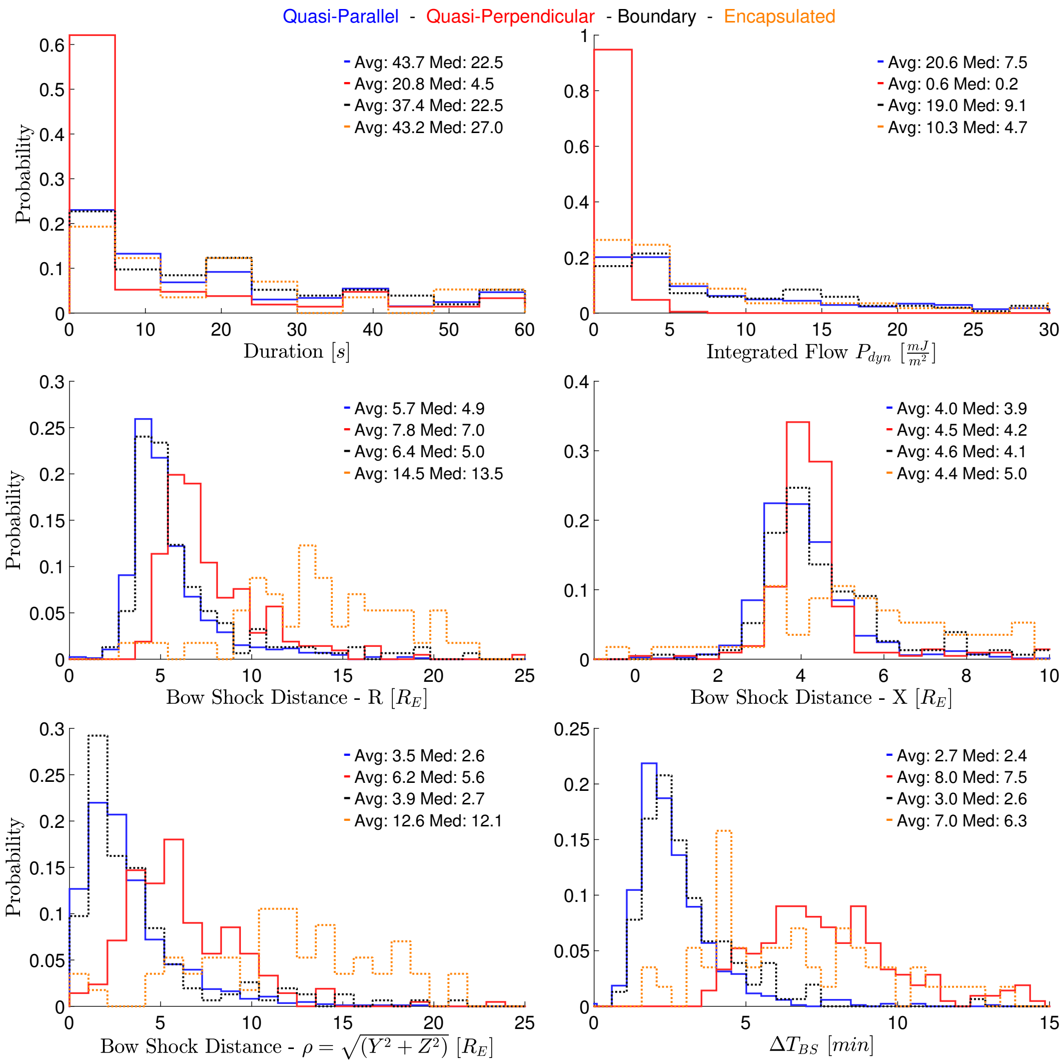


**Figure 5.** Histograms showing distributions, average and median values for scale sizes and for positions compared to an estimated point of origin at the bow shock. $\Delta T_{BS}$ describes the time that was estimated for the jet to arrive to MMS from its origin point at the bow shock.

The average and median jet duration of the main class jets is found to be 39 and 18 seconds respectively. This result is similar to the average of $\sim 30$ seconds that has been reported in previous studies (Němeček et al., 1998; Savin et al., 2012; Archer & Horbury, 2013; Plaschke et al., 2013). As shown in Figure 5, Qpar and encapsulated jets have a slightly longer duration than boundary jets, while the Qperp jets have a much shorter duration, with the majority of them consisting of only 1 data point. It should be noted that the duration of encapsulated jets is biased to appear longer by their definition (Table 2), since shorter jets would be classified as Qpar.

In Figure 5, when looking at the dynamic pressure integrated over the jet (Eq. (15)) we see a consistent picture where the shorter duration along with the lower dynamic pressure make the Qperp jets much weaker in comparison to the rest of the jet classes. On average the rest of the jets seem to be similar with the Qpar and boundary jets, again having very similar properties. The distance from the bow shock (Eq. (9)) is quite different for each class. While boundary and Qpar have similar relative positions, the Qperp jets are found further inside the magnetosheath. This difference is more visible when looking at the distance on the $yz$ plane from the bow shock. Encapsulated jets are also found at a much higher radial distance ($R$) from the bow shock, again with the $\rho$ component having much higher values than the rest of the classes. It should be noted that, Qperp jets are found to occur primarily under low-velocity solar wind conditions. As a result, the bow shock model used for those cases, generates a bow shock further away from the Earth than for the cases of Qpar and Boundary jets. Finally, the time that it took each jet to reach the MMS is much different as expected. Qpar and boundary jets need on average $\sim$ 3 minutes while the much slower Qperp jets require much more at around $\sim$ 8 minutes. Encapsulated jets also take a long time to reach MMS from their origin point ($\sim$ 7 min) but in contrast to Qperp jets, this is due to their large distance that they have to cover rather than their velocity.

Figure 6 shows that the temperature profiles are quite different between each class. On average, the temperature is lower on Qperp jets ($\sim$ 100 eV) compared to the rest of the jets ($\sim$ 300 eV). The difference of both $T_{\perp}$ and $T_{||}$ compared to the background is negative and very similar between boundary and Qpar jets. On the other hand, it is around zero for Qperp jets and positive for the encapsulated jets. Most of the observed differences are expected due to the nature of the magnetosheath region and from the definition of each class. As mentioned in the previous subsection, encapsulated and boundary jets have a very different background magnetosheath. Therefore, a direct comparison between each class can be misleading, especially in the case of the highly variant temperature measurements.

An interesting difference regarding the mean absolute magnetic field appears in Figure 6. Qpar jets have on average, a smaller mean absolute magnetic field than the rest of the classes ($\langle |B|_{mean} \rangle \sim 25$ nT). Encapsulated jets have almost twice as high values while the mean absolute magnetic field of Qperp and boundary jets' is in between, at $\langle |B|_{mean} \rangle \sim 30$ nT.

The difference in the mean absolute magnetic field ($\Delta |B|_{mean}$) is higher in Qpar and boundary jets compared to Qperp and encapsulated jets. Specifically, Qpar and boundary jets have a bigger absolute magnetic field than their background magnetosheath. On the other hand, Qperp jets have on average a slightly smaller magnetic field although the actual values range for individual events change significantly ($\Delta |B|_{mean} \in [-10, 10]$ nT).

Figure 7 shows how plasma (thermal) and magnetic pressures vary between each class along with their ratio ($\beta$ parameter). For all the classes, the maximum plasma pressure is on average higher than the maximum magnetic pressure. However, when looking at the difference values, comparing with the background, the Qpar and the boundary jets have higher maximum magnetic pressure ($\Delta P_{magnetic,max}$) than maximum plasma pressure ($\Delta P_{plasma,max}$). On the other hand, Qperp and encapsulated jets still have a higher maximum thermal pressure difference than maximum magnetic pressure difference. Looking at the maximum magnetic pressure and its difference to the background can also be directly interpreted as a measurement of the maximum absolute magnetic field. This information shows us that although from the previous histograms (Figure 6), the average magnetic field ($|B|_{mean}$) is higher in the case of Qperp jets, the maximum ($|B|_{max}$) values are higher in the Qpar and boundary cases. This could originate from the higher duration of Qpar jets, along with the higher time resolution of the FGM data compared to the FPI. These two factors can allow very high magnetic field values to oc-

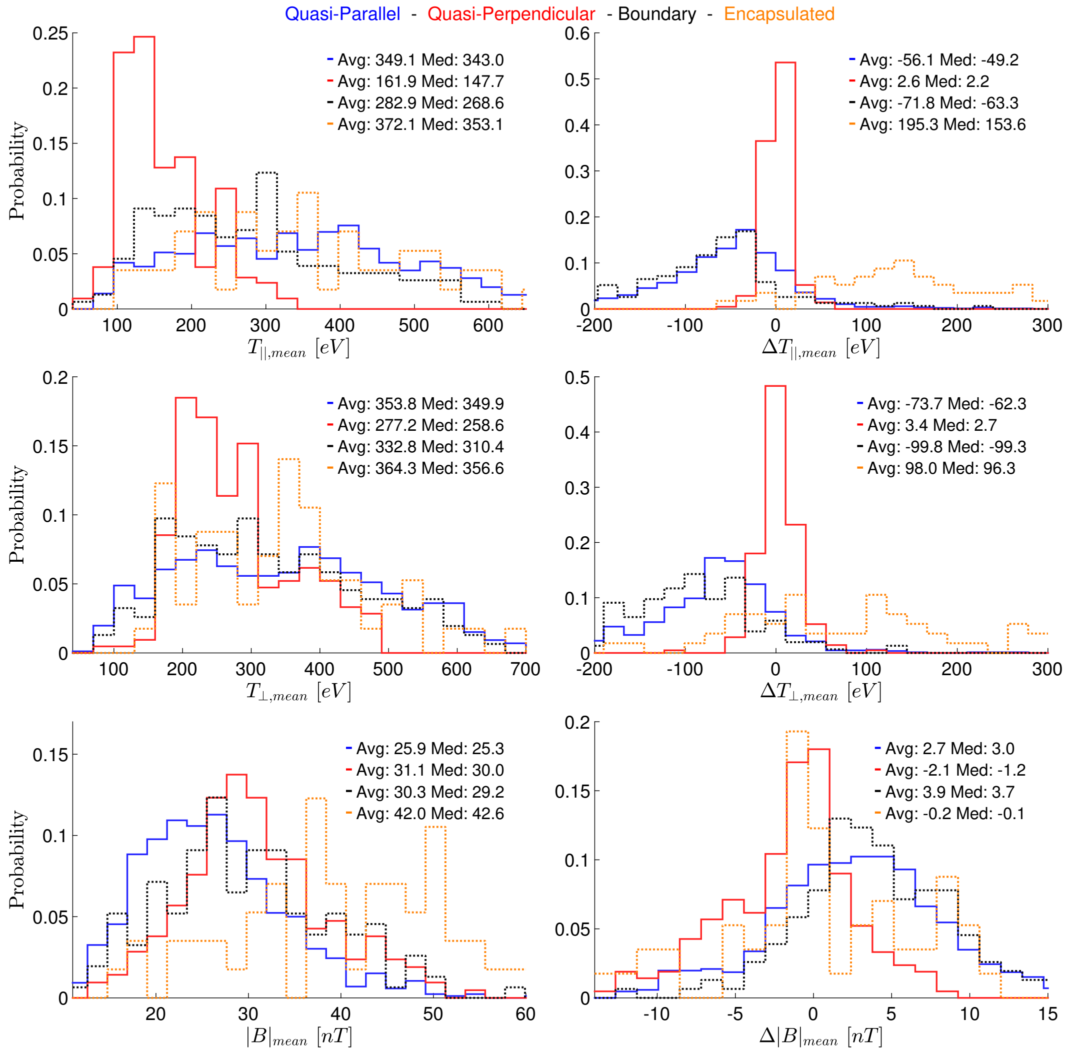


**Figure 6.** Histograms showing distributions, average and median values for the average values of temperature and absolute magnetic field.

cur within a jet period since in principle $|B|$ can have a higher variance in the quasi-parallel environment. The behavior of the $\beta$ parameter is consistent with the previous results. While it is higher for the Qpar and boundary classes, it is on average smaller than that of the background plasma around the jets. On the other hand, encapsulated and Qperp jets have on average smaller beta values but still maintain a positive difference when compared to the background.

Specifically, average beta values appear to be closer to unity for the Qperp and encapsulated cases, while they are on average higher ($\langle\beta_{qpar}\rangle \sim 10$ , $\langle\beta_{boundary}\rangle \sim 6$) for the other classes. When looking at the difference to the background, it appears that Qpar and boundary jets have a negative beta difference ($\Delta\beta < 0$). This could indicate that magnetic pressure has a larger effect in the jet than in the surrounding magnetosheath plasma.

The velocity components of each class are shown in Figure 8. Here, we present the absolute velocity for the $y$ and $z$ component. This was done because all jets and especially encapsulated jets had a distribution that produced an average velocity close to zero,

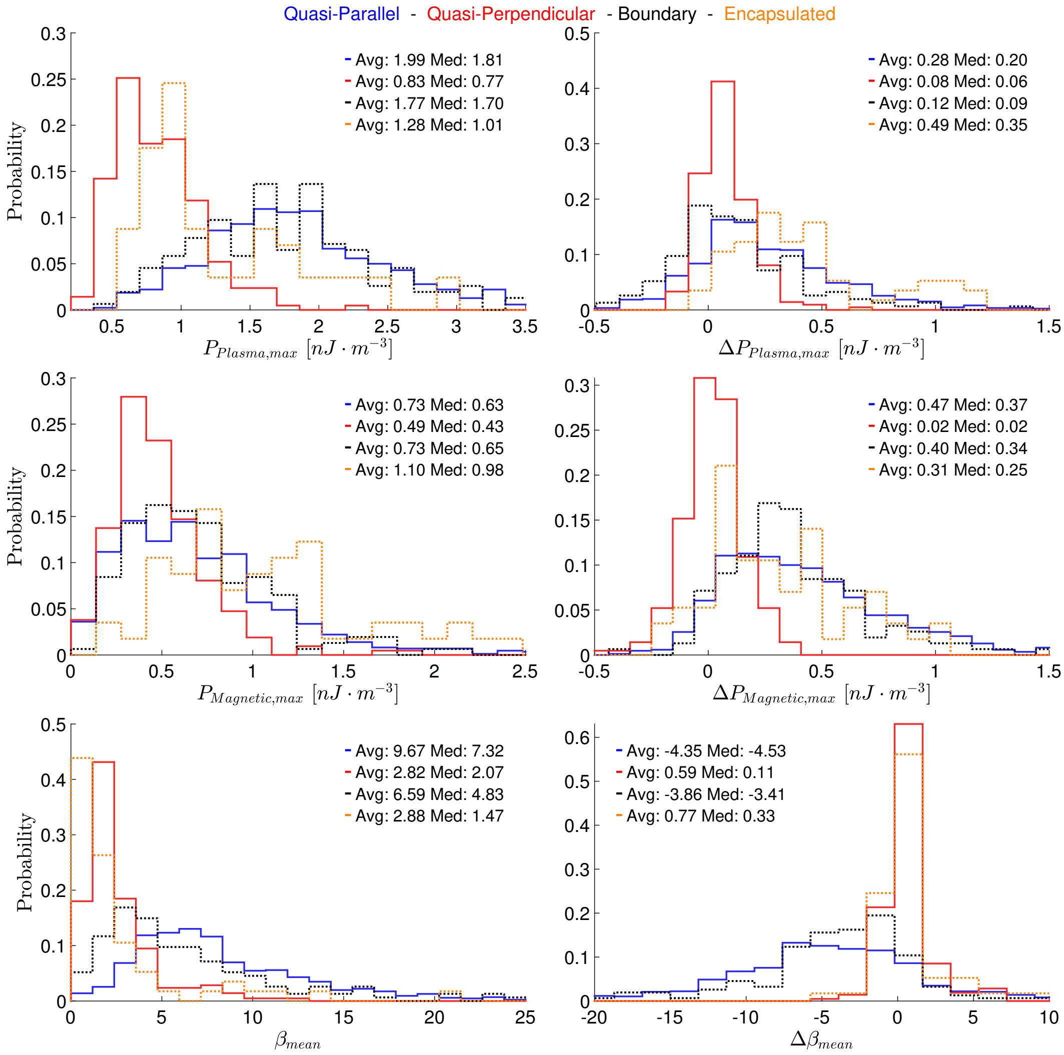


**Figure 7.** Histograms showing distributions, average and median values for the maximum plasma pressure, the maximum magnetic pressure and the mean $\beta$ parameter.

in both components, due to equally frequent jets exhibiting a high negative and positive $V_{y,z}$. As a result, providing a histogram without the absolute values would limit the information of each class, and would not contribute to a meaningful comparison.

As expected, almost every jet has a dominating negative (earthward) $x$ component, with the Qperp jets on average having smaller values on every velocity component compared to the other classes. Furthermore, Qperp jets seem to have very similar velocities in all three components which are different from the rest of the classes that tend to have a more significant imbalance between components. An interesting difference can be seen in the encapsulated jets where the dominant component of their velocity is surprisingly $V_y$ and $V_z$. The same effect can be seen when we look at the absolute difference ($|V_{jet} - V_{MSH}|$), where the difference to the background seems to be higher for the Qpar and boundary jets than Qperp jets, while encapsulated exhibit values much higher than the rest of the classes.

Finally, in Figure 9, directional information and rotation angles of the magnetic field and the velocity are given. As expected the $yz$ plane velocity ($V_\rho$) is much higher

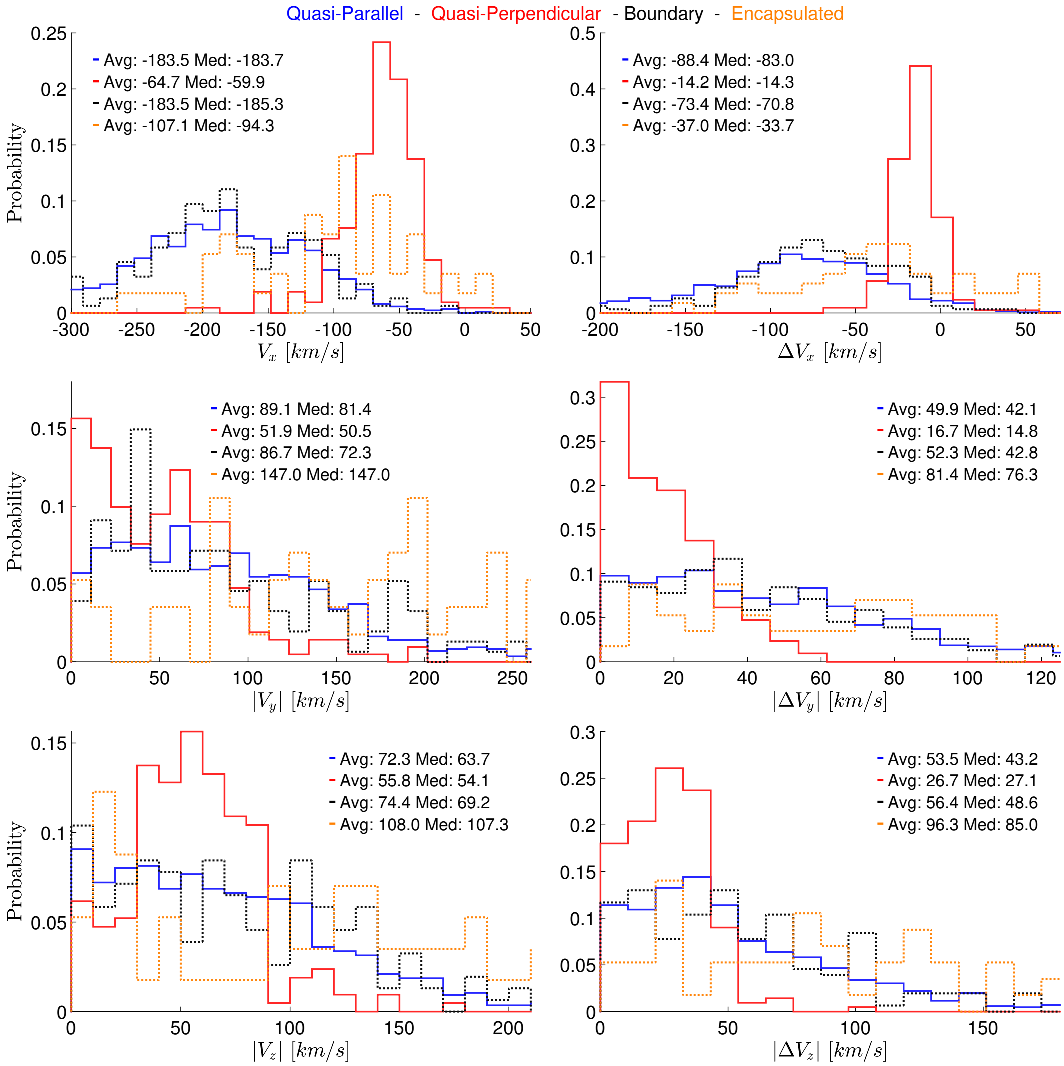


**Figure 8.** Histograms showing distributions, average and median values for each velocity component at $|V|_{max}$.

for the encapsulated jets compared to the other three classes. This can also be seen when calculating the angle between the jet's velocity and $x$ axis (Eq. (12)), in which we can see that Qpar and Boundary jets show similar behavior, while Qperp jets have on average a higher angle and encapsulated jets the highest. This picture is consistent when comparing to the background plasma in which Qpar and boundary jets show a net decrease in the angle while Qperp and encapsulated show a net increase. Looking at the magnetic field rotation angle (Eq. (13)), there seems to be a significant difference between the Qperp jets and the other classes. Qperp have on average a very small ($\sim 6°$) difference while the rest of the classes have on average higher values, particularly the Qpar jets. Considering velocity rotation angles (Eq. (14)), Qperp jets exhibit the least changes, although all classes seem to have similar statistical values and distributions.

It should be noted that since both velocity and magnetic field rotation angles describe the changes between the plasma before and after jet, the results are heavily affected by the duration of the jet. Specifically, it is expected that jets with a shorter du-

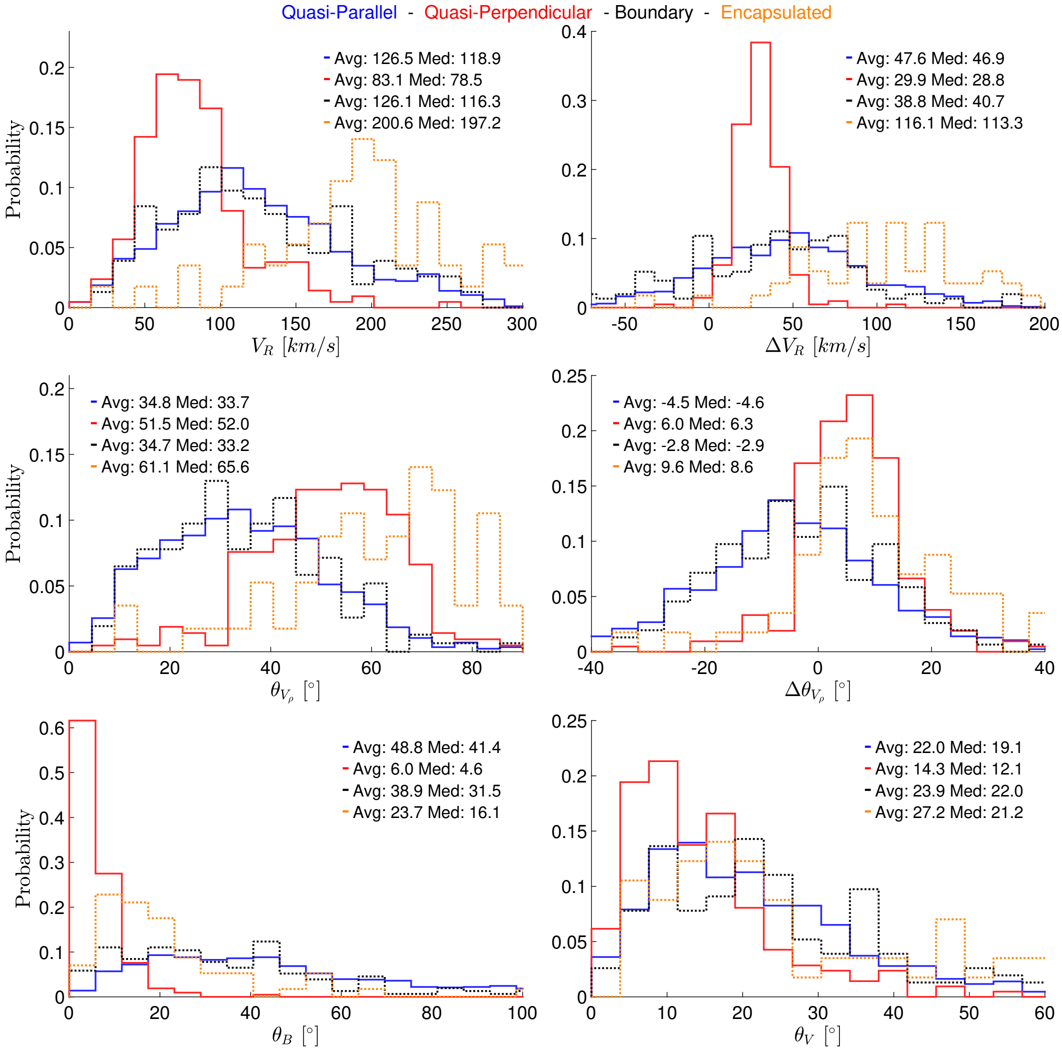


**Figure 9.** Histograms showing average and median values for directional information and other calculated angles.

ration such as Qperp jets would statistically have a smaller angle change since measurements taken are spatially and temporally closer to each other.

### 4.2 Relation Between Jet Properties

In this subsection, we will report on some observations on correlations between different jet properties.

There is a moderate correlation between the magnetic field rotation angle ($\theta_B$) and both the maximum dynamic pressure ($P_{max}$) and the difference of maximum dynamic pressure compared to the background ($\Delta P_{max}$).

Specifically, regardless of the way we calculated the magnetic field rotation angle, we found a moderate correlation with both quantities using Spearman's coefficient, $\rho_{Sp,All} = 0.43{\pm}0.02$. Considering only subsolar jets this correlation was increased, reaching $\rho_{Sp,Subsolar} = 0.6 \pm 0.05$.

A possible interpretation could be that the jets distort the magnetic field lines that are embedded in the plasma in front of them. On weaker jets such as in the majority of Qperp jets (Figures 4 and 9) this effect would be hardly visible since we see the dynamic pressure being an order of magnitude less compared to the other classes and the magnetic field rotation angle is also close to zero. On the other hand, on jets that on average have a higher velocity and density gain, magnetic field vector seems to be different in the plasma in front and behind the jet. To investigate this possible link further, we looked at class-specific correlation coefficients. For the classes of Qperp and Qpar jets, it was found that the correlation is almost non-existent ($\rho_{Sp,Subsolar,||,\perp} = 0.1 \pm 0.05$.), as a result, we conclude that the correlation was caused by the different properties of each class causing an artificial correlation that does not necessarily represent a physical property. The above result emphasizes the importance of classifying jets that physically occur in different environments before drawing any strong conclusions.

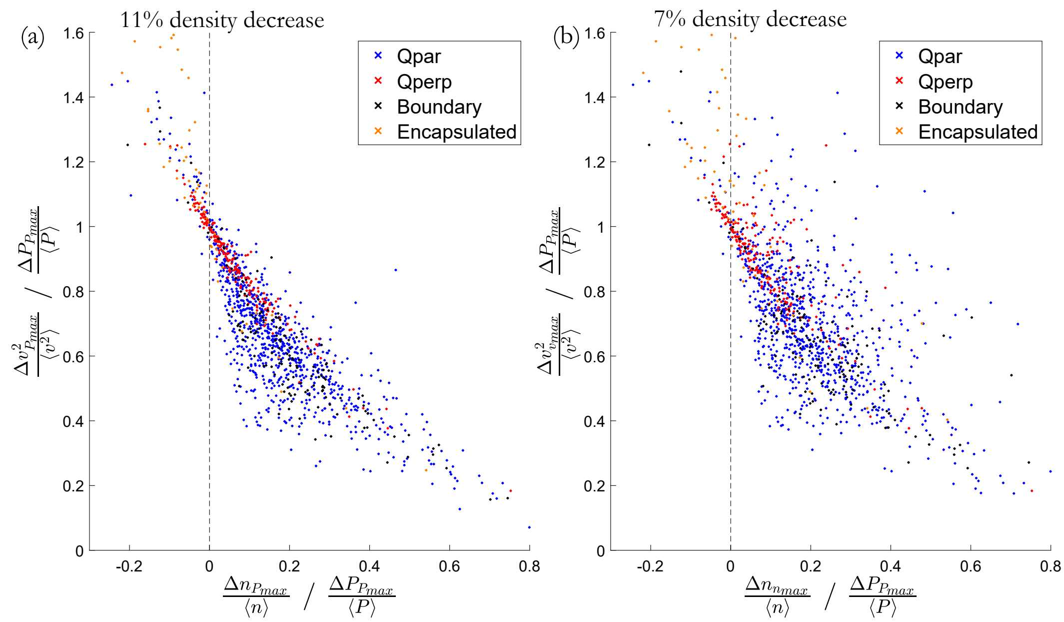


**Figure 10.** (a): Relative difference in density and velocity at the time of maximum $P_{dyn}$. (b): Relative difference in density and velocity for the maximum value of each quantity, measured within the jet period.

In Figure 10, a comparison between the density and the velocity squared difference normalized by the total dynamic pressure gain is shown, similar to Figure 3 of Archer and Horbury (2013). Figure 10(a) shows the relative change in density and velocity with measurements taken at the point of maximum dynamic pressure. In Figure 10(b) however, the difference is taken by using the measurements of maximum density, velocity and dynamic pressure for each quantity. As shown in Figure 10, the majority of the jets have a combination of velocity and density increase, contributing to the overall dynamic pressure enhancement. For the Qpar and boundary cases, less than 0.5% jets are purely velocity driven, exhibiting a density decrease compared to the background plasma. On the other hand, Qperp jets can have a decrease in density up to 22% and encapsulated jets up to 68% of the times, making their dynamic pressure to mainly originate from a velocity increase. More information regarding the velocity and density distribution of each class can be found in Table 4. As expected, most of the jets regardless of their class exhibit an increase in both density and velocity when comparing to the background magnetosheath. This result shows that the increased frequency of Qpar and boundary jets

**Table 4.** Velocity and density distribution of jets that exhibit a dynamic pressure increase. First values are based on the maximum quantity met within jet's duration and values in parenthesis are derived from the density and velocity value found at $P_{max}$.

| Class | Velocity Decrease (%) $V_{V_{max}}(V_{P_{max}})$ | Density Decrease (%) $n_{n_{max}}(n_{P_{max}})$ |
|---|---|---|
| All | 1.6 (1.8) | 6.9(10.9) |
| Main Classes | 0 (0) | 7.3(10.8) |
| Quasi - Parallel | 0 (0) | 2.9(5.23) |
| Quasi - Perpendicular | 0 (0) | 15.6(22.3) |
| Boundary | 0 (0) | 3.9(5.2) |
| Encapsulated | 0 (0) | 50.1(68.4) |

can be at least partially attributed to density enhancements taking place, while being insignificant or even absent in the case of Qperp jets.

When comparing our results to earlier studies, we find that they are quite similar. In particular, we find that depending on the normalization technique, $7 - 11\%$ of the jets exhibit a relative decrease in density with their increase in dynamic pressure being caused by a very high enhancement of absolute velocity. Plaschke et al. (2013) found 10.5% using a different jet criterion, while Archer et al. (2012) using essentially the same criterion as this work found 18%. In the main classes, we find no cases exhibiting a velocity decrease as shown in Figure 10 and Table 4. In order to see if there are any jets showing a velocity decrease we searched the full jet database ($n = 8499$). The only cases with a velocity decrease were 158 jets from which 151 have been classified as "Border" jets, found too close to either the magnetopause or the bow shock. Therefore, since any calculation averaging over different plasma regions is statistically unreliable, we exclude them. Careful examination on the rest of the 7 cases showed that they were jets that occurred very close to another jet but not close enough to fulfill the criteria of jet combining (Eq. (3)). As a result, we conclude that there are no jets showing a relative velocity decrease at their maximum dynamic pressure measurement.

In Figure 11 we present two different types of cross-plots. In subplots (a) and (c), plots of the difference in maximum density ($\Delta n_{max}$) against difference in maximum magnetic field ($\Delta|B|_{max}$) with and without solar wind normalization are shown. This was done in order to test a hypothesis that connects SLAMS to the generation of Qpar jets (Archer et al., 2012; Karlsson et al., 2015) We, therefore, search for some kind of correlation between the density increase and the magnetic field increase since SLAMS have such a correlation (Schwartz & Burgess, 1991; Behlke et al., 2003). In the sub-figures (b) and (d) we similarly investigate the difference of maximum velocity ($\Delta V_{max}$) against the difference in minimum temperature ($\Delta T_{min}$). This was done to see if a correlation can be found that could support the mechanism proposed by Hietala et al. (2009) that associates jets with ripples of the quasi-parallel bow shock. As discussed and shown in earlier studies, it is expected that the background plasma surrounding the ripple-generated jet would be more de-accelerated and would, in turn, have a higher temperature compared to the jet flow created by passing through a ripple of the bow shock, undergoing less de-acceleration, and heating (Hietala & Plaschke, 2013; Plaschke et al., 2013).

As shown in Figure 11(a,c), for the quasi-perpendicular jets, there is no significant correlation between the difference in maximum magnetic field ($\Delta B_{max}$) and the difference in maximum density ($\Delta n_{max}$). However, in the case of quasi-parallel jets, there is a moderate monotonic relationship between the two quantities. Spearman's rho value ($\rho_{Sp}$) for the quasi parallel case is $\rho_{Sp,a,||} = 0.57$ and $\rho_{Sp,c,||} = 0.55$, whereas for the

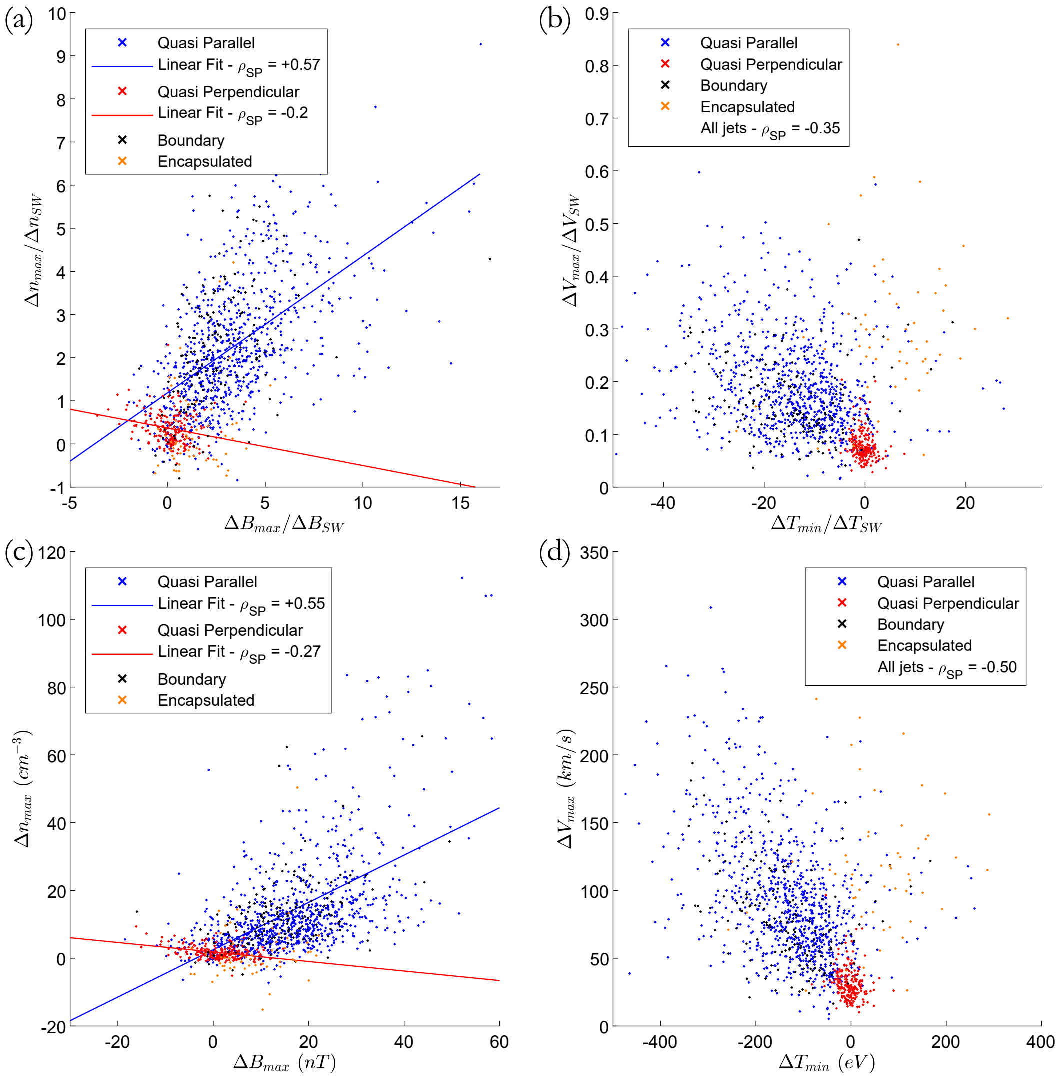


**Figure 11.** (a): $\Delta n_{max}$ against $\Delta|B|_{max}$ normalized over solar wind data. Linear regression lines are shown for visual guidance, for the Qpar (blue) and Qperp (red) cases. (b): $\Delta V_{max}$ against $\Delta T_{min}$ normalized over solar wind data. (c): $\Delta n_{max}$ against $\Delta|B|_{max}$. Linear regression lines are shown for visual guidance, for the Qpar (blue) and Qperp (red) cases. (d): $\Delta V_{max}$ against $\Delta T_{min}$. In all figures every point represents a jet while the color shows its class.

quasi-perpendicular jets is $\rho_{Sp,a,\perp} = -0.2$ and $\rho_{Sp,c,\perp} = -0.27$. For all the jets together, a total correlation of $\rho_{Sp,a} = 0.66$ and $\rho_{Sp,c} = 0.63$ is reached.

These results support the idea that a subset of quasi-parallel jets may originate from a SLAMS interacting with bow-shock ripples as described by Karlsson et al. (2015). Further support of this mechanism is shown when looking back at the general characteristics of each class. In Figure 4 it is shown that $\Delta n_{max}$ is an order of magnitude higher for the Qpar jets compared to the Qperp. Furthermore, in Figure 6, Qpar jets exhibit on average a positive difference on the average absolute magnetic field compared to the Qperp jets that do not. Maximum magnetic pressure and average $\beta$ values shown in Figure 7 also support SLAMS since Qpar and boundary jets have not only a higher magnetic pressure than Qperp jets, but also a higher value than their surrounding plasma.

It should be noted, however, that the anti-correlation observed for Qperp jets can not be directly explained through any known mechanism. The observed anti-correlation should be treated with caution since it was only found for the ”best cases” of Qperp jets (Table 3). When we look at the whole body of Qperp jets the observed correlation disappears.

In Figure 11(b,d) a weak/moderate linear correlation between the difference in minimum temperature ($\Delta T_{min}$) and the difference in maximum absolute ion velocity ($\Delta V_{max}$) is shown. Correlation coefficients are found to be $\rho_{Sp,b} = -0.35$ and $\rho_{Sp,d} = -0.5$ when looking at the whole body of the jets. While looking exclusively at Qpar jets, we find $\rho_{Sp,b,||} = -0.28$ and $\rho_{Sp,d,||} = -0.43$. On the other hand, when looking at Qperp jets, we find correlation coefficients of $\rho_{Sp,b,\perp} = -0.24$ and $\rho_{Sp,d,\perp} = -0.23$.

All main class jets have a small to medium anti-correlation relation between the temperature and the velocity difference within the jet period (Figure 11(b,d)). As discussed previously, we can interpret this result as indirect support of a mechanism that is based on the bow shock ripple idea (Hietala et al., 2009; Hietala & Plaschke, 2013). This result is also supported by the general properties shown in Figure 6, where for Qpar jets there is a larger difference between the temperature of the background magnetosheath plasma and the jet. Finally, it has been recently found that similar ripples can be found also at the quasi-perpendicular bow shock which could mean that the generation mechanism of these jets is of the same nature (Johlander et al., 2016). Although the majority of the jets seems to have a medium anti-correlation that could support Hietala's mechanism (Hietala et al., 2009; Hietala & Plaschke, 2013), we cannot say the same for the quasi-perpendicular where the anti-correlation is weaker. It should be noted, however, that due to the very small duration of the jets, there is usually only one measurement for the temperature and the velocity. Therefore, there is a higher uncertainty regarding this result compared to the other classes.

Finally, based on the differences between thermal and magnetic pressure shown in Figure 7, we investigate possible relationships with other jet properties.

Regarding the difference in maximum magnetic pressure, there is a moderate to strong correlation with the total integrated dynamic pressure $\rho_{Sp,All} = 0.72$. Although this result could be interpreted in terms of SLAMS similarly to the analysis of Figure 11, all the components of Eq. (15) are correlated including the difference in maximum absolute velocity $\rho_{Sp,All} = 0.59$ and the duration $\rho_{Sp,All} = 0.62$ of the jet. This result is unexpected and can be considered an indication that magnetic forces play a more important role than previously thought. Qpar jets have similar correlations, while Qperp jets are also alike, apart from the same anti-correlation shown in Figure 11, regarding the density difference and $\Delta|B|$. It should be noted that this effect appears on all the jets and not only in the Boundary jets as initially speculated

However, when looking at each class exclusively, the results show that the effect decreases significantly for the duration and velocity for both Qpar and Qperp jets $\rho_{Sp} \sim 0.2$. The correlation (when taking all classes together) seems to have been artificially created because in jets with higher velocities (and duration) it is relatively easier to measure magnetic field in higher values due to its high variance. Surprisingly, the only effect that seems to be robust and even enhanced when taking average quantities is the correlation between the density difference ($\Delta n_{mean,max}$) and the absolute magnetic field difference ($\Delta|B|_{mean,max}$). Specifically, Qpar jets have a positive correlation in all four possible combination, $\rho_{Sp,||} \in [0.3, 0.7]$. Similarly, the anti-correlation of the Qperp jets remains, $\rho_{Sp,\perp} \in [-0.28, -0.65]$. Once more, we should point out that the correlation found in the Qpar jets remains high when looking at all the Qpar jets rather than the 'best cases' (Table 3). On the other hand, the observed anti-correlation almost fully disappears for the Qperp jets.

From this result, we conclude that the magnetic field seems to play an important role in forming the density profile of each class, possibly explained through SLAMS mechanism. The correlation found on other jets' properties although less consistent, could still indicate that magnetic fields could have a more important role regarding the velocity and duration of the jet.

An interesting difference was also found when investigating the difference in both the maximum and the average thermal plasma pressure difference ($\Delta P_{th,mean,max}$).

Qpar jets when investigated with the maximum differences in density and thermal pressure, have a moderate correlation $\rho_{Sp,||} = 0.35$. However, when we take average values for density or thermal pressure, this correlation disappears fully. On the other hand, as discussed previously, density changes are heavily correlated with the magnetic pressure of the Qpar jets. This result shows that the changes in temperature are more important than the changes in density in deriving the thermal pressure difference. On the other hand, Qperp jets have a high correlation of density change and thermal pressure $\rho_{Sp,\perp} = [0.5, 0.7]$. This indicates that the contribution of density change in thermal pressure difference is more important than the temperature difference for the Qperp jets.

## 5 Discussion and Conclusion

We have investigated the properties of an extensive dataset of magnetosheath jets ($n = 8499$) using MMS, and classified them in different categories based on the angle $\theta_{Bn}$ between IMF and the bow shock's normal vector. The general properties found were in agreement with earlier studies. In particular, our dataset contains jets with an average duration of $\sim 30$ seconds, similar to what has been reported in other studies (Němeček et al., 1998; Savin et al., 2012; Archer & Horbury, 2013; Plaschke et al., 2013). Their dynamic pressure enhancement was found to be in most cases due to both a velocity and density enhancement (Amata et al., 2011; Archer & Horbury, 2013; Plaschke et al., 2013; Karlsson et al., 2015). There was no clear case exhibiting a velocity decrease compared to the background magnetosheath, while for all the jets, velocity appears to always be smaller than associated solar wind measurements. Finally, on average, most of the jets that can be appropriately normalized, have a lower temperature compared to their background. This is in principle expected for a flow that has been less heated and de-accelearted from the bow shock interaction as shown in previous studies (Savin et al., 2008; Amata et al., 2011; Hietala et al., 2012; Archer et al., 2012; Plaschke et al., 2013, 2018). We have additionally made a number of new observations that are discussed in the following subsections.

### 5.1 Quasi-Parallel and Quasi-Perpendicular Jets

The results of our study show that quasi-parallel jets are considerably more frequent than quasi-perpendicular jets. Specifically, similar to recent results (Vuorinen et al., 2019), they were found to occur $\sim 5{-}10$ times more frequently than quasi-perpendicular jets. On average they have a dynamic pressure around 3.5 nPa, with the majority of them exhibiting both a density and a velocity increase. Their density increase shows a significant correlation with the absolute magnetic field increase ($\rho_{Sp} = 0.5 \pm 0.2$) indicating a possible association of at least a subset of them to SLAMS. A moderate anti-correlation was found between the maximum velocity difference ($\Delta V_{max}$) and the minimum temperature difference ($\Delta T_{min}$). This could be interpreted as a relatively weak support of the bow shock ripple mechanism. Furthermore, the high magnetic field values and variance found could indicate possible wave activity that may contribute to their properties. Finally, most of the quasi-parallel jets are earthward with very high velocities, making them very interesting candidates to investigate phenomena such as jet-triggered magnetopause reconnection or other magnetosphere coupling phenomena.

Quasi-perpendicular jets have a much smaller dynamic pressure than the rest of the classes and their dynamic pressure is mainly due to a velocity increase rather than a density enhancement. Their duration is significantly smaller (median: 4.5 seconds per jet) and their total integrated dynamic pressure is more than an order of magnitude lower than the corresponding values of the other jet types. While their existence is clear according to the criterion used, their importance regarding magnetospheric influence is to be questioned.

Their properties, when compared to Qpar jets, suggest that either a different mechanism or a smaller scale version of Qpar generation mechanism causes their creation. The density differences, can be in principle, attributed to the absence of SLAMS that are believed to occur only in the ion foreshock generated under quasi-parallel bow shock. On the other hand, we hypothesize that their low velocities compared to the other classes could be the result of one or more of the following effects. The jet criterion used (Eq. (1)) is fulfilled more easily during low dynamic pressure conditions compared to high dynamic pressure ones. As a result, there might be an observational bias causing MMS to observe primarily jets that occur under low-velocity solar wind conditions. Secondly, there might be a link between the actual solar wind conditions and the IMF orientation, in which slower solar wind flow could be attributed to IMF conditions where $B_y$ and $B_z$ components are more dominant. Finally, assuming that ripples in the quasi-perpendicular bow shock (Johlander et al., 2016) are related to the jets generation mechanism, maybe the smaller amplitude and scales of these ripples can affect the jet properties. Specifically, the smaller amplitude of Qperp ripples can create a geometry in which the Qperp jet undergo a larger breaking compared to the case of the sharper (more inclined) transitions of the ripples associated with Qpar jets. The different scales could also contribute to the short duration of the Qperp jets. The smaller scale ripples would benefit the creation of smaller flow structure than larger ones regarding their tangential size. In turn, when these flows meet MMS under some random angle, their measured duration would be significantly smaller.

To investigate the possibility of an observational bias, we examine the distributions of the solar wind velocities associated with and without jets. We find that indeed, on average the associated solar wind velocities are much higher for the quasi-parallel jets ($\langle V_{SW,||Jets} \rangle \approx$ 495 km/s) than for the quasi-perpendicular jets ($\langle V_{SW,\perp Jets} \rangle \approx 400$ km/s). However, when observing the total solar wind distribution, solar wind velocities associated with the Qperp bow shock ($\langle V_{SW,\perp} \rangle \approx 425$ km/s) have smaller difference to the solar wind velocities associated with Qpar bow shock ($\langle V_{SW,||} \rangle \approx 445$ km/s). As a result, while the difference of the solar wind conditions associated to jets is around $\sim 100$ km/s, for the solar wind, it is only $\sim 20$ km/s.

From the discussion above, we can conclude that all four effects (absence of SLAMS, observational bias, differences in SW, smaller scale ripples) could in principle take place and contribute to the differences that were observed between the jet properties of Qpar and Qperp jets.

The distance from the bow shock appears to be different for quasi-parallel and quasi-perpendicular jets, with Qpar jets occurring on average closer to the bow shock than Qperp jets. It should be noted, that this result might be artificial since (as discussed above) it is possible that as Qperp jets are found more frequently during slow solar wind speed conditions, this can affect that result. In particular, Qperp jets occur for lower solar wind velocities and as a result the bow shock will be further towards the sun. i.e. when MMS measures the Qperp jet, the distance between bow shock and jets will be larger than for Qpar jets. As a result, our statistics of the bow shock positions may be affected by observing a particular subset of jets, associated with low-velocity solar wind conditions.

Finally, Qperp jets have a velocity increase that is on average equally distributed between each velocity component (Figure 8) and more importantly, velocities of the Qperp jets seem to have a different angle compared to the background flow as shown in Figure 9. This result could mean several things. One possibility would be that the observed subset of Qperp jets originating from low-velocity solar wind can have a specific, predetermined velocity orientation. On the other hand, Qpar jets may also originate from a particular high velocity solar wind subset which has another distinct, yet different, velocity orientation. Another possible explanation is that Qperp jets have travelled a longer distance in the magnetosheath region compared to Qpar jet (see Figure 5) which could cause the Qperp jet to have a less distinct difference compared to the background magnetosheath flow.

Qpar and Qperp jets exhibit differences regarding their beta values and how magnetic and thermal pressure contribute to their properties. While a higher $\beta$ is found in the Qpar jets, when subtracting the contribution of the background magnetosheath, another picture arises. Qpar jets have $\Delta\beta_{mean} < 0$, which means that the magnetic pressure is maybe more important for the jets than for the surrounding magnetosheath. In Qperp jets, however, the jet has a $\Delta\beta_{mean} \sim 0$. Specifically, while the overall region (magnetosheath) is basically dominated in both cases by gas dynamics ($\beta_{mean} > 1$), the Qpar jets are maybe controlled relatively more by magnetic pressure and the Qperp jets are governed slightly more by thermal pressure.

These changes in *beta* parameter can be interpreted via three different mechanisms. First of all, SLAMS originating from the ion foreshock increase the magnetic field of Qpar jets and create an initial increase on the magnetic pressure compared to the Qperp cases where SLAMS are absent. Secondly, the background magnetosheath regions have differences in density, temperature and possibly magnetic field, which could contribute to different result both in their total $\beta$ parameter but also when subtracting the background ($\Delta\beta$). Finally, If we assume that Qperp jets indeed travel longer distances from the bow shock than Qpar jets, the differences in $\beta$ might provide insight regarding the fate of the jets as they travel in the magnetosheath. Qperp jets are created further away and may have reached a later stage of their existence in which both the magnetosheath background flow including the jet is mainly guided equally by the gas dynamics and the background magnetic field. In this case, the weaker Qperp jets are maybe seen in a later stage of their magnetosheath propagation in which their already weak properties make them relatively insignificant to the magnetospheric environment.

### 5.2 Quasi-Parallel and Boundary Jets

As for the boundary jets, we did not find any significant differences in their properties compared to Qpar jets, indicating a very similar phenomenon. Although some differences can be observed between the two classes, almost all of them can be attributed to the different properties of the background magnetosheath before and after the jet. Specifically, for the boundary jets, by definition, the plasma surrounding them is of both Qpar and Qperp nature. Some authors have speculated that maybe boundary jets are driven primarily by magnetic field tension forces and therefore point to a different origin than the rest of the classes (Archer et al., 2012; Karlsson et al., 2018). However, our results clearly show, both the magnetic field components (Figure 5) and the magnetic field rotation angles (see Figure 9) being very similar to the quasi-parallel jets. Also, all their basic properties are almost identical. Their dynamic pressure and its components have very similar distributions and average values to these of Qpar jets (see Figure 4). The temperature and the magnetic field profiles along with their distance from bow shock are also alike (see Figures 5 & 6). Moreover, the correlations between the different quantities were very similar to the ones found in Qpar jets.

We therefore suggest that Qpar and boundary jets form a superset of jets with very similar properties and possibly same origin. It is unlikely that different physical mechanisms may generate two subsets of jets with so similar statistical properties. One of the things that was not tested however, is how frequent these jets occur compared to how often we exhibit a switch between Qpar and Qperp magnetosheath. A detailed analysis of that could point out a frequency difference if any.

To summarize, our results suggest that the quasi-parallel and the boundary jets are the classes connected to jet-related phenomena, such as the throat aurora (Han et al., 2017; Wang et al., 2018), magnetopause reconnection (Hietala et al., 2018) and possibly the radiation belts (Turner et al., 2012; Xiang et al., 2016). Finally, both Qpar and boundary jets exhibit high earthward velocities and duration, making them important to investigate magnetosphere coupling phenomena and geoeffective properties.

### 5.3 Encapsulated Jet Origin Hypothesis

From the observations of the encapsulated jets, we can infer that there are at least two distinct subgroups of jets that are perhaps associated to a different creation mechanism.

The first ones are those that exhibit a positive $V_x$ or that have an extremely small velocity, $|V_x| < 20$ km/s. These rare cases (7/57) could be the result of a plasma reflection from the magnetopause. This picture is also consistent with the general trend that encapsulated jets are found closer to the magnetopause than the rest of the jets, and could also explain why some of the jets have positive $V_x$ since these reflected flows could in principle point to any direction when measured by MMS at any point of their lifetime.

For the encapsulated jets that have a strong enough negative $V_x$ (50/57), a possible scenario is that they are associated with a rotation of the IMF, generating a Qpar and a Qperp plasma environment sequentially. The jet is created in the quasi-parallel plasma environment, having a higher velocity, it gradually overtake the quasi-perpendicular plasma allowing the formation of a region of Qpar plasma 'encapsulated' within the Qperp magnetosheath plasma to be measured by MMS.

Another possible explanation which we propose as our main hypothesis is that encapsulated jets are a subset of quasi-parallel jets, created at the flanks of the bow shock. This picture provides a direct explanation to the similarities that are generally found between Qpar and encapsulated jets (high velocity increase, low temperature anisotropy, distinct high energy ion population, etc.). After investigating the associated solar wind conditions it was found that encapsulated jets appear when the IMF is dominated by its $y$ component. This would result in a quasi-perpendicular bow shock close to the subsolar region of the magnetosheath. At the same time, an ion foreshock is formed in the flanks allowing the same effects that apply to Qpar jets to take place. This picture allows a mechanism similarly described to the bow shock ripple mechanism (Hietala et al., 2009; Hietala & Plaschke, 2013) to generate jets. We hypothesize that the orientation of the normal vector ($\hat{n}$) close to the flanks, can deflect the downstream flow into a dominant $yz$ velocity component that encapsulated jets appear to have on average. Finally, the definition we used for encapsulated jets, to be Qpar plasma surrounded by Qperp, creates an observational bias, since in the case that encapsulated jets remain in quasi-parallel environment, they would simply be classified as Qpar jets.

As a result, we believe that encapsulated jets are quasi-parallel jets generated at the flanks, that travel a long distance and are finally measured by MMS in quasi-perpendicular background magnetosheath. This hypothesis is illustrated in Figure 12.

The presented hypothesis also explains how a few encapsulated jets exhibit velocities higher than the upstream solar wind conditions associated to them. First we have an error at the propagation of solar wind measurements to the bow shock. The data we are using are propagated to the bow shock nose and as a result there is a time lag er-

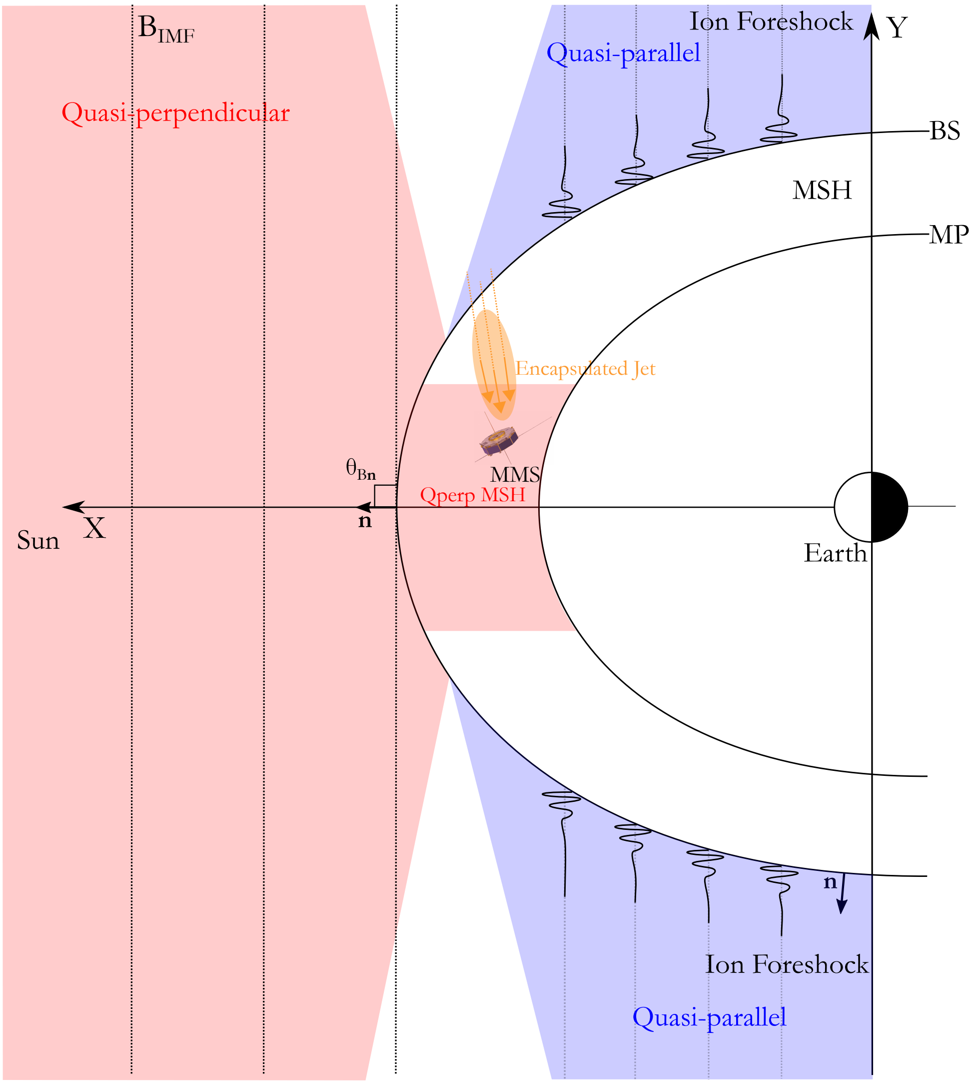


**Figure 12.** Visualization of encapsulated jet creation model. We assume a purely $y$ component IMF which creates a large region of quasi-perpendicular angles around the subsolar point while the flanks are of quasi-parallel nature. The creation of the jet is done at the flanks of bow shock where ion foreshock is generated. Sequentially, MMS measures the jet travelling from the flanks towards the subsolar point, while the surrounding plasma is characterized by a constant flow originating from the quasi-perpendicular bow shock (red shaded area).

ror for the solar wind that arrives at the flanks of the bow shock. Secondly, such a jet, originating from the flanks of the bow shock, would take long time to reach the observation point (MMS). As a result, the solar wind measurement association done for each jet is more unreliable for these cases.

None of the presented mechanism can directly explain why encapsulated jets have a density distribution similar to the quasi-perpendicular jets. In Figure 4 we can see that there is little to no density increase within an encapsulated jet. This effect can be seen more clearly when calculating the difference of the mean density for the jet ($\Delta n = \langle n \rangle_{jet} - \langle n \rangle_{5min}$). Doing so we find that on average there is a density decrease in an encapsulated jet ($\Delta n_{mean} = -1.7$ nPa). This is also supported by the distribution of the relative difference in velocity and density that can be seen in Figure 10 and in Table 4. There, we see several encapsulated jets showing a density decrease.

One mechanism that can explain the density decrease is if expansion takes place while the jet travels through the magnetosheath region. This could also help to explain the difference of the densities found in Qperp jets that are also found at larger distances from the bow shock at that due to their low velocities have travelled for a longer time in the magnetosheath. To investigate this hypothesis, we search for correlations between the radial ($R$) distance from the bow shock origin point, and the difference in maximum density ($\Delta n_{max}$). Doing so for the subsolar jets ($n = 289$), it was found that they are moderately anti-correlated, $\rho_{Sp,subsolar} = -0.5 \pm 0.05$. It should be noted that this effect remained when looking at class specific correlations for the case of subsolar encapsulated ($\rho_{Sp,subsolar,enc} = -0.7$) and subsolar Qpar jets ($\rho_{Sp,subsolar,||} = -0.27$). It however almost fully disappeared when investigating Qperp and boundary jets. After careful examination, it was realized that boundary subsolar jets of our dataset were contained within a very short range of bow shock distances possibly explaining the absence of any correlation. On the other hand, while subsolar Qperp jets had a wide range of radial distance ($R$), they had a very small range of density difference possibly affecting the correlation result. These results could possibly be interpreted as a weak indication of expansion taking place while the jets travel in the magnetosheath region, although for drawing any stronger conclusions more in depth analysis is required.

Another possibility could be that a diffusion process due to magnetic reconnection or Kelvin-Helmholtz instabilities at the boundary between the jet and the background flow occurs, reducing the density of the jet as it travels in the magnetosheath.

To summarize, the encapsulated jets are found on average further away from the bow shock, they have on average a very large velocity in the $yz$ plane while they usually exhibit a density drop. Their exact nature still needs to be determined. If their origin is confirmed, they can provide vital information regarding the evolution of the jet since we hypothesize that they are flows that while having a high velocity they have undergone an expansion which lowers their density compared to Qpar jets. As a result, such a jet, if created at the flanks of the bow shock, it could create a very interesting case study to investigate the dynamic evolution of its properties from its creation at the bow shock until its observation.

### 5.4 Generation Mechanisms of Jets

As mentioned in the previous subsections, the bow shock ripple mechanism (Hietala et al., 2009; Hietala & Plaschke, 2013) is supported indirectly by Figure 6 where we can see that the difference between the temperature of the jet and the background is negative in Qpar jets, indicating that the jet flow could be less de-accelerated than the background flow by passing through a bow shock ripple. Furthermore, in Figure 11(b,d), it was shown that there is a moderate correlation between the maximum velocity difference and the minimum temperature difference. However, it is very hard to draw any important conclusion since the correlations are not robust enough. Although it seems that jet generation could be related to the ripples of the bow shock, there could be more factors that influence their generation that may or may not be connected to this mechanism. A more direct way to evaluate the bow shock ripple mechanism would be to analyze the jets that appear close to the bow shock and compare with those found closer to the magnetopause. Doing so, one can quantify how well the initial properties of the jets are explained through the ripple mechanism and whether this effect gradually diminishes as the jets travel towards the Earth. For the shake of completeness, we looked at jets close to the subsolar point and to the bow shock and we found that the anti-correlation increases ($\rho_{Sp,subsolar} \approx -0.65 \pm 0.1$). However, more careful analysis is needed to investigate this effect.

We find support for the SLAMS-related mechanism (Karlsson et al., 2015) when looking at the differences of maximum magnetic pressure (Figure 7) and most importantly at the correlations shown in Figure 11(a,c) between $\Delta n_{max}$ and $\Delta|B|_{max}$. We conclude that SLAMS play an important role contributing to the dynamic pressure enhancement of some of the Qpar jets which can explain some of the differences in the properties of Qperp jets where SLAMS do not occur, since they are a phenomenon typically associated with the quasi-parallel bow shock.

Both the bow shock ripple and SLAMS-associated mechanisms are therefore supported and appear to be key elements of jet creation. However, it could be the case that there are more contributing mechanisms to the formation and composition of jets. As previously discussed, the magnetic field is quite different for each class, while it is persistently correlated to several basic properties of most jets. It is possible that the IMF frozen into the solar wind has a more important impact on the jets than previously thought. The high variance of the magnetic field shown in various jets could indicate instabilities and wave activity that may play a role in establishing the jet properties. We believe that more careful investigation regarding phenomena such as acceleration mechanisms, instabilities and wave interactions might lead to a more complete answer regarding the origin of the jets.

Finally, there have been several cases where the correlations shown in all the jets disappear when investigating class-specific correlations. This can be interpreted as a validation of the classification, showing that the derived classes indeed represent a very similar yet distinct physical phenomenon. However, it also indicates that, on large scale statistics that include phenomena of diverse nature, correlation-driven conclusions can be unreliable and require further investigation. With the use of advanced techniques originating from probability and information theory (e.g. mutual information) along with careful classification, sampling and interpretation, we might in the future be able to derive stronger conclusions regarding the origin and generation of jets.

We close this work saying that we are aiming to make some final refinements and make the presented dataset publicly available in the near future. If anyone is however interested in using the dataset for their research sooner, they are encouraged to contact the corresponding author for more information.

## Appendix A Classification Thresholds and Stages

For the classification process we use the following physical quantities:

Averaged "very high" differential energy flux
$$F_{VH} = \frac{1}{3}\sum_{i}^{30:32} F_i \tag{A1a}$$

Averaged "high" energy differential flux
$$F_{H} = \frac{1}{3}\sum_{i}^{27:29} F_i \tag{A1b}$$

Averaged "medium" energy differential flux
$$F_{M} = \frac{1}{5}\sum_{i}^{18:22} F_i \tag{A1c}$$

Summed magnetic field standard deviation
$$\sigma(\mathbf{B}) = \sum_{j}^{1:3} \sigma(B_j) \tag{A1d}$$

Temperature anisotropy
$$Q = \frac{T_\perp}{T_\parallel} - 1 \tag{A1e}$$

Total high / medium energy flux ratio
$$C = \frac{F_{VH} + F_H}{F_M} \tag{A1f}$$

**Table A1.** Quantities and thresholds used for each stage of the classification procedure. Number in the subscript indicates the average time window in seconds used for each quantity. Prime quantities ($X^{'}$) indicate a re-scaling of the quantity (min-max normalization: ($X \in [0, 1]$). Average quantities ($\langle X \rangle$), are computed starting from 1 minute before the jet up to 1 minute after. Finally, $\Gamma \in [0.05, 0.1]$.

| Stages | Quasi - Parallel | Quasi - Perpendicular |
|---|---|---|
| 1, 2a, 2b | $F_{VH,30} > 2.9 \cdot 10^5$<br>$F_{H,30} > 4 \cdot 10^5$<br>$\sigma(\vec{B})_{60} > 14$<br>$Q_{30} < 0.4$<br>$C > 0.1$ | $F_{VH,30} < 2.6 \cdot 10^5$<br>$F_{H,30} < 3 \cdot 10^5$<br>$\sigma(\vec{B})_{60} < 13$<br>$Q_{30} > 0.45$<br>$C < 0.075$ |
| 3a 3b, 3c | $F_{VH,0} > 3.0 \cdot 10^5$<br>$F_{H,0} > 4.1 \cdot 10^5$<br>$\sigma(\vec{B})_{30} > 14$<br>$Q_0 < 0.3$ | $F_{VH,0} < 2.5 \cdot 10^5$<br>$F_{H,0} < 2.9 \cdot 10^5$<br>$\sigma(\vec{B})_{30} < 12$<br>$Q_0 > 0.35$ |
| 4, 5, 6 | $F^{'}_{VH,0} > \langle F^{'}_{VH,0} \rangle + \Gamma$<br>$F^{'}_{H,0} > \langle F^{'}_{H,0} \rangle + \Gamma$<br>$\sigma(\vec{B})^{'}_{30} > \langle \sigma(\vec{B})^{'}_{30} \rangle + \Gamma$<br>$Q^{'}_0 < \langle Q^{'}_0 \rangle - \Gamma$ | $F^{'}_{VH,0} < \langle F^{'}_{VH,0} \rangle - \Gamma$<br>$F^{'}_{H,0} < \langle F^{'}_{H,0} \rangle - \Gamma$<br>$\sigma(\vec{B})^{'}_{30} < \langle \sigma(\vec{B})^{'}_{30} \rangle - \Gamma$<br>$Q^{'}_0 > \langle Q^{'}_0 \rangle + \Gamma$ |

Where, $i$ is the energy channel of the ion energy spectrum and $j$ is the component of the magnetic field in GSE coordinates. We choose to not multiply with the energy difference ($\Delta E$) for every bin of the energy flux in order to avoid weighting each flux component differently when averaging over. Very high energy flux represents ions of $16 - 28$ keV, high energy is of $7 - 12$ keV and medium is between 0.55 and 1.7 keV.

The classification process holds several stages, thresholds, and methods. In principle, we vary the thresholds of each quantity on every stage according to the values shown in Table A1. It should be noted that not all the thresholds have to be met in order for a classification to be made. Necessary criteria include $F_{VH}, F_H$, and $\sigma(\vec{B})$, while the others serve mainly as quality indicators. Furthermore, the actual classification is being done by separating the jet into three periods as explained in the main text (pre-jet, jet, post-jet). Then we apply these thresholds and we classify each period depending on what the majority of the data points have been classified into. During each stage, we vary the time period of pre-jet and post-jet slightly in order to allow the algorithm to take under consideration the different time scales that can occur on every jet.

## Appendix B Verification Procedure - Fine Parameter Searching

In order to verify the accuracy of our classification scheme we created a test set of 180 jets (that we identified by visual inspection) that represent our 4 main classes as shown in Table 2, or that has been categorized as ”unclassified”. This set has been thoroughly checked by visual inspection in order to represent a characteristic sample of the desired classes that we are looking to find.

To create an initial classification scheme, we implemented some coarse threshold values and techniques which we evaluated using the test set in order to quantify the accuracy and the misclassification ratio of our code. The first accuracy results can be seen in Table B1.

**Table B1.** Initial accuracy before fine parameter searching.

| Stage | Q-Par (%) | | Q-Perp (%) | | Bound. (%) | | Encaps. (%) | | Unknown (%) |
|---|---|---|---|---|---|---|---|---|---|
| | Acc. | Mis. | Acc. | Mis. | Acc. | Mis. | Acc. | Mis. | Mis. |
| 1 | 94.7 | 0 | 36.4 | 0 | 10.8 | 0 | 4 | 4 | 0 |
| 2 | 94.7 | 0 | 39.4 | 0 | 10.8 | 0 | 20 | 4 | 0 |
| 3 | 94.7 | 0 | 84.9 | 0 | 10.8 | 0 | 20 | 4 | 11.9 |
| 4 | 94.7 | 2.6 | 84.9 | 3.1 | 89.2 | 0 | 80 | 4 | 45.3 |

**Table B2.** Final accuracy after fine parameter searching & last modifications. Emphasized text shows the stages that were found to work ideally for each class.

| Stage | QPar (%) | | QPerp (%) | | Bound. (%) | | Encaps. (%) | | Unknown (%) |
|---|---|---|---|---|---|---|---|---|---|
| | Acc. | Mis. | Acc. | Mis. | Acc. | Mis. | Acc. | Mis. | Mis. |
| 1 | **100** | **0** | 36.4 | 0 | 13.5 | 0 | 4 | 4 | 0 |
| 2 | 100 | 0 | 39.4 | 0 | 13.5 | 0 | 24 | 4 | 2.4 |
| 3 | 100 | 0 | **90.9** | **0** | 13.5 | 0 | 24 | 4 | 11.9 |
| 4 | 100 | 0 | 90.9 | 0 | 89.2 | 0 | 76 | 4 | 26.2 |
| 5 | 100 | 0 | 90.9 | 0 | **91.9** | **0** | **80** | **4** | 26.2 |
| 6 | 100 | 0 | 90.9 | 0 | 91.9 | 0 | 80 | 6 | 28.6 |

Based on these results, we adjusted the thresholds several times, slightly changed the procedure and introduced 2 more stages. We then repeat this process until a maximum value of accuracy and a minimum value of misclassification was reached for the majority of the classes. The final result of the classification scheme regarding its accuracy can be seen in Table B2.

From the final accuracy results, we decided that the sample size and the quality of quasi-perpendicular and quasi-parallel jets is optimal when we are using only 1 stage of our scheme. On the other hand, it is possible to increase the number of jets of quasi-perpendicular case until stage 3 relatively safely. Moving on, for the boundary and encapsulated jets due to the complexity of their structure, we increase the number of stages utilized by the algorithm to 5. This ensures that our statistics have a large enough sample size that even the possibility of a few misclassification cases will not significantly affect the final results.

Afterwards, we manually changed the class of approximately $\sim 10\%$ of the jets that failed to be automatically classified in their class. The final step was to manually verify the cases that we believed were misclassified from the underrepresented classes (boundary & encapsulated). After doing so, we found no significant difference between the characteristics of the automatically derived database and the manually cleaned one. However, since we want to ensure the scientific value of our results, we cross-validated the dataset via manual inspection for the cases that the accuracy results were lower and the number of jets was limited (boundary & encapsulated). This process provided the final dataset shown in Table 3, which was then used for the main analysis of this work.

## Acknowledgments

We thank the MMS team for providing data and support `https://omniweb.gsfc.nasa.gov/form/omni_min.html`. Furthermore, we acknowledge use of NASA/GSFC's Space Physics Data Facility's OMNIWeb service, and OMNI data. OMNI High-resolution data are available through `https://omniweb.gsfc.nasa.gov/form/omni_min.html`. This work was supported by Swedish National Space Board (SNSA grant 90/17).

## References

Amata, E., Savin, S., Ambrosino, D., Bogdanova, Y., Marcucci, M., Romanov, S., & Skalsky, A. (2011). High kinetic energy density jets in the earth's magnetosheath: A case study. *Planetary and Space Science*, *59*(7), 482–494.

Anderson, B. J., Fuselier, S. A., Gary, S. P., & Denton, R. E. (1994). Magnetic spectral signatures in the earth's magnetosheath and plasma depletion layer. *Journal of Geophysical Research: Space Physics*, *99*(A4), 5877–5891.

Angelopoulos, V., Kennel, C., Coroniti, F., Pellat, R., Kivelson, M., Walker, R., … Gosling, J. (1994). Statistical characteristics of bursty bulk flow events. *Journal of Geophysical Research: Space Physics*, *99*(A11), 21257–21280.

Archer, M., Hietala, H., Hartinger, M., Plaschke, F., & Angelopoulos, V. (2019). Direct observations of a surface eigenmode of the dayside magnetopause. *Nature communications*, *10*.

Archer, M., & Horbury, T. (2013). Magnetosheath dynamic pressure enhancements: occurrence and typical properties. In *Annales geophysicae* (Vol. 31, p. 319).

Archer, M., Horbury, T., & Eastwood, J. (2012). Magnetosheath pressure pulses: Generation downstream of the bow shock from solar wind discontinuities. *Journal of Geophysical Research: Space Physics*, *117*(A5).

Behlke, R., André, M., Buchert, S. C., Vaivads, A., Eriksson, A. I., Lucek, E. A., & Balogh, A. (2003). Multi-point electric field measurements of short large-amplitude magnetic structures (slams) at the earth's quasi-parallel bow shock. *Geophysical research letters*, *30*(4).

Burch, J., Moore, T., Torbert, R., & Giles, B. (2016). Magnetospheric multiscale overview and science objectives. *Space Science Reviews*, *199*(1-4), 5–21.

Case, N., & Wild, J. (2012). A statistical comparison of solar wind propagation delays derived from multispacecraft techniques. *Journal of Geophysical Research: Space Physics*, *117*(A2).

Chao, J., Wu, D., Lin, C.-H., Yang, Y.-H., Wang, X., Kessel, M., … Lepping, R. (2002). Models for the size and shape of the earth's magnetopause and bow shock. In *Cospar colloquia series* (Vol. 12, pp. 127–135).

Chen, S.-H., Kivelson, M. G., Gosling, J. T., Walker, R. J., & Lazarus, A. J. (1993). Anomalous aspects of magnetosheath flow and of the shape and oscillations of the magnetopause during an interval of strongly northward interplanetary magnetic field. *Journal of Geophysical Research: Space Physics*, *98*(A4), 5727–5742.

Formisano, V., & Hedgecock, P. (1973). Solar wind interaction with the earth's magnetic field: 3. on the earth's bow shock structure. *Journal of Geophysical Research*, *78*(19), 3745–3760.

Fuselier, S. A. (2013). Suprathermal ions upstream and downstream from the earth's bow shock. In *Solar wind sources of magnetospheric ultra-low-frequency waves* (p. 107-119). American Geophysical Union (AGU). Retrieved from `https://agupubs.onlinelibrary.wiley.com/doi/abs/10.1029/GM081p0107` doi: 10.1029/GM081p0107

Fuselier, S. A., Anderson, B. J., Gary, S. P., & Denton, R. E. (1994). Inverse correlations between the ion temperature anisotropy and plasma beta in the earth's quasi-parallel magnetosheath. *Journal of Geophysical Research: Space Physics*, *99*(A8), 14931–14936.

Giacalone, J., & Jokipii, J. R. (2007). Magnetic field amplification by shocks in turbulent fluids. *The Astrophysical Journal Letters*, *663*(1), L41.

Gosling, J., Asbridge, J., Bame, S., Paschmann, G., & Sckopke, N. (1978). Observations of two distinct populations of bow shock ions in the upstream solar wind.

*Geophysical Research Letters*, *5*(11), 957–960.
Gunell, H., Wieser, G. S., Mella, M., Maggiolo, R., Nilsson, H., Darrouzet, F., … others (2014). Waves in high-speed plasmoids in the magnetosheath and at the magnetopause. In *Annales geophysicae* (Vol. 32, pp. 991–1009).
Gutynska, O., Sibeck, D., & Omidi, N. (2015). Magnetosheath plasma structures and their relation to foreshock processes. *Journal of Geophysical Research: Space Physics*, *120*(9), 7687–7697.
Han, D.-S., Hietala, H., Chen, X.-C., Nishimura, Y., Lyons, L. R., Liu, J.-J., … Yang, H.-G. (2017). Observational properties of dayside throat aurora and implications on the possible generation mechanisms. *Journal of Geophysical Research: Space Physics*, *122*(2), 1853-1870. doi: 10.1002/2016JA023394
Hietala, H., Laitinen, T. V., Andréeová, K., Vainio, R., Vaivads, A., Palmroth, M., … Rème, H. (2009). Supermagnetosonic jets behind a collisionless quasiparallel shock. *Physical review letters*, *103*(24), 245001.
Hietala, H., Partamies, N., Laitinen, T. V., Clausen, L. B. N., Facskó, G., Vaivads, A., … Lucek, E. A. (2012). Supermagnetosonic subsolar magnetosheath jets and their effects: from the solar wind to the ionospheric convection. *Annales Geophysicae*, *30*(1), 33–48. Retrieved from https://www.ann-geophys.net/30/33/2012/ doi: 10.5194/angeo-30-33-2012
Hietala, H., Phan, T., Angelopoulos, V., Oieroset, M., Archer, M., Karlsson, T., & Plaschke, F. (2018). In situ observations of a magnetosheath high-speed jet triggering magnetopause reconnection. *Geophysical Research Letters*, *45*(4), 1732–1740.
Hietala, H., & Plaschke, F. (2013). On the generation of magnetosheath high–speed jets by bow shock ripples. *Journal of Geophysical Research: Space Physics*, *118*(11), 7237–7245.
Johlander, A., Schwartz, S. J., Vaivads, A., Khotyaintsev, Y. V., Gingell, I., Peng, I. B., … Burch, J. L. (2016, Oct). Rippled quasiperpendicular shock observed by the magnetospheric multiscale spacecraft. *Phys. Rev. Lett.*, *117*, 165101. Retrieved from https://link.aps.org/doi/10.1103/PhysRevLett.117.165101 doi: 10.1103/PhysRevLett.117.165101
Karlsson, T., Brenning, N., Nilsson, H., Trotignon, J.-G., Vallières, X., & Facsko, G. (2012). Localized density enhancements in the magnetosheath: Three-dimensional morphology and possible importance for impulsive penetration. *Journal of Geophysical Research: Space Physics*, *117*(A3).
Karlsson, T., Kullen, A., Liljeblad, E., Brenning, N., Nilsson, H., Gunell, H., & Hamrin, M. (2015). On the origin of magnetosheath plasmoids and their relation to magnetosheath jets. *Journal of Geophysical Research: Space Physics*, *120*(9), 7390–7403.
Karlsson, T., Liljeblad, E., Kullen, A., Raines, J. M., Slavin, J. A., & Sundberg, T. (2016). Isolated magnetic field structures in mercury's magnetosheath as possible analogues for terrestrial magnetosheath plasmoids and jets. *Planetary and Space Science*, *129*, 61–73.
Karlsson, T., Plaschke, F., Hietala, H., Archer, M., Blanco-Cano, X., Kajdic, P., … Gershman, D. J. (2018). Investigating the anatomy of magnetosheath jets-mms observations. In *Annales geophysicae.*
King, J., & Papitashvili, N. (2005). Solar wind spatial scales in and comparisons of hourly wind and ace plasma and magnetic field data. *Journal of Geophysical Research: Space Physics*, *110*(A2).
Lavraud, B., Borovsky, J., Ridley, A., Pogue, E., Thomsen, M., Rème, H., … Lucek, E. (2007). Strong bulk plasma acceleration in earth's magnetosheath: A magnetic slingshot effect? *Geophysical Research Letters*, *34*(14).
Lin, Y., Swift, D., & Lee, L. (1996). Simulation of pressure pulses in the bow shock and magnetosheath driven by variations in interplanetary magnetic field direction. *Journal of Geophysical Research: Space Physics*, *101*(A12), 27251–27269.

Luhmann, J., Russell, C., & Elphic, R. (1986). Spatial distributions of magnetic field fluctuations in the dayside magnetosheath. *Journal of Geophysical Research: Space Physics*, *91*(A2), 1711–1715.

Mailyan, B., Munteanu, C., & Haaland, S. (2008). What is the best method to calculate the solar wind propagation delay? In *Annales geophysicae* (Vol. 26, pp. 2383–2394).

Merka, J., Szabo, A., Narock, T., King, J., Paularena, K., & Richardson, J. (2003). A comparison of imp 8 observed bow shock positions with model predictions. *Journal of Geophysical Research: Space Physics*, *108*(A2).

Myers, J. L., Well, A. D., & Lorch Jr, R. F. (2013). *Research design and statistical analysis*. Routledge.

Němeček, Z., Šafránková, J., Přech, L., Sibeck, D., Kokubun, S., & Mukai, T. (1998). Transient flux enhancements in the magnetosheath. *Geophysical research letters*, *25*(8), 1273–1276.

Omidi, N., Zhang, H., Sibeck, D., & Turner, D. (2013). Spontaneous hot flow anomalies at quasi-parallel shocks: 2. hybrid simulations. *Journal of Geophysical Research: Space Physics*, *118*(1), 173–180.

Palmroth, M., Hietala, H., Plaschke, F., Archer, M., Karlsson, T., Blanco-Cano, X., … others (2018). Magnetosheath jet properties and evolution as determined by a global hybrid-vlasov simulation. In *Annales geophysicae.*

Plaschke, F., & Glassmeier, K.-H. (2011). Properties of standing kruskal-schwarzschild-modes at the magnetopause. In *Annales geophysicae* (Vol. 29, pp. 1793–1807).

Plaschke, F., & Hietala, H. (2018). Plasma flow patterns in and around magnetosheath jets. In *Annales geophysicae* (Vol. 36, pp. 695–703).

Plaschke, F., Hietala, H., Angelopoulos, V., et al. (2013). Anti-sunward high-speed jets in the subsolar magnetosheath. In *Annales geophysicae.*

Plaschke, F., Hietala, H., Archer, M., Blanco-Cano, X., Kajdič, P., Karlsson, T., … others (2018). Jets downstream of collisionless shocks. *Space Science Reviews*, *214*(5), 81.

Pollock, C., Moore, T., Jacques, A., Burch, J., Gliese, U., Saito, Y., … others (2016). Fast plasma investigation for magnetospheric multiscale. *Space Science Reviews*, *199*(1-4), 331–406.

Retinò, A., Sundkvist, D., Vaivads, A., Mozer, F., André, M., & Owen, C. (2007). In situ evidence of magnetic reconnection in turbulent plasma. *Nature Physics*, *3*(4), 235.

Russell, C., Anderson, B., Baumjohann, W., Bromund, K., Dearborn, D., Fischer, D., … others (2016). The magnetospheric multiscale magnetometers. *Space Science Reviews*, *199*(1-4), 189–256.

Savin, S., Amata, E., Zelenyi, L., Budaev, V., Consolini, G., Treumann, R., … others (2008). High energy jets in the earth's magnetosheath: Implications for plasma dynamics and anomalous transport. *JETP letters*, *87*(11), 593–599.

Savin, S., Amata, E., Zelenyi, L., Lutsenko, V., Safrankova, J., Nemecek, Z., … others (2012). Super fast plasma streams as drivers of transient and anomalous magnetospheric dynamics. In *Annales geophysicae* (Vol. 30, p. 1).

Schwartz, S. J., & Burgess, D. (1991). Quasi-parallel shocks: A patchwork of three-dimensional structures. *Geophysical Research Letters*, *18*(3), 373–376.

Schwartz, S. J., Burgess, D., Wilkinson, W. P., Kessel, R. L., Dunlop, M., & Lühr, H. (1992). Observations of short large-amplitude magnetic structures at a quasi-parallel shock. *Journal of Geophysical Research: Space Physics*, *97*(A4), 4209–4227.

Stone, C. E., M. Frandsen, A., Mewaldt, R., Christian, E., Margolies, D., Ormes, J., & Snow, F. (1998, 07). The advanced composition explorer mission. *Space Science Reviews*, *86*, 1-22. doi: 10.1023/A:1005082526237

Turc, L., Fontaine, D., Savoini, P., Hietala, H., & Kilpua, E. K. J. (2013). A comparison of bow shock models with cluster observations during low alfvén mach number magnetic clouds. *Annales Geophysicae*, *31*(6), 1011–1019. Retrieved from https://www.ann-geophys.net/31/1011/2013/ doi: 10.5194/angeo-31-1011-2013

Turner, D. L., Shprits, Y., Hartinger, M., & Angelopoulos, V. (2012). Explaining sudden losses of outer radiation belt electrons during geomagnetic storms. *Nature Physics*, *8*(3), 208.

Vuorinen, L., Hietala, H., & Plaschke, F. (2019). Jets in the magnetosheath: Imf control of where they occur. In *Annales geophysicae* (Vol. 37, pp. 689–697).

Wang, B., Nishimura, Y., Hietala, H., Lyons, L., Angelopoulos, V., Plaschke, F., … Weatherwax, A. (2018). Impacts of magnetosheath high-speed jets on the magnetosphere and ionosphere measured by optical imaging and satellite observations. *Journal of Geophysical Research: Space Physics*, *123*(6), 4879–4894.

Wilson III, L. (2016). Low frequency waves at and upstream of collisionless shocks. *Low-frequency waves in space plasmas*, 269–291.

Xiang, Z., Ni, B., Zhou, C., Zou, Z., Gu, X., Zhao, Z., … others (2016). Multi-satellite simultaneous observations of magnetopause and atmospheric losses of radiation belt electrons during an intense solar wind dynamic pressure pulse. *Annales Geophysicae (Online)*, *34*(LA-UR-15-27237).

Zhang, H., Sibeck, D., Zong, Q.-G., Omidi, N., Turner, D., & Clausen, L. (2013). Spontaneous hot flow anomalies at quasi-parallel shocks: 1. observations. *Journal of Geophysical Research: Space Physics*, *118*(6), 3357–3363.